DOI: 10.1002/chem.200700601

Conformational Effects of Bay Substituents on Optical, Electrochemical and Dynamic Properties of Perylene Bisimides: Macrocyclic Derivatives as Effective Probes

Peter Osswald and Frank Würthner*[a]

Dedicated to Professor Waldemar Adam on the occasion of his 70th birthday

Abstract: A series of diagonally and laterally bridged regioisomeric macrocycles based on 1,6,7,12-tetraaryloxy-substituted perylene bisimides (APBIs) have been synthesized and characterized. The different orientations of the aryloxy residues, that is, horizontal or perpendicular to the perylene core, in the regioisomeric macrocycles have been elucidated by NMR spectroscopy, and the dynamic properties of the laterally bridged regioisomers have been investigated by temperature-dependent NMR measurements. The influence of the different orientations of the aryloxy substituents on the electrochemical properties of APBIs is demonstrated by cyclic voltammetry, which reveals that a perpendicular orientation of the aryloxy residues relative to the perylene core leads to a substantial decrease of the LUMO energy level of the perylene bisimide electrophore. The optical properties of the regioisomeric macrocycles have been determined by UV/Vis and fluorescence spectroscopy. It has been shown that the diagonally bridged macrocycles exhibit optical properties that differ significantly from those of an open-chain reference compound, whereas the optical properties of the laterally bridged isomers resemble those of the reference system. This demonstrates that unrestricted aryloxy substituents prefer the lateral conformation in solution. Solvent-dependent fluorescent properties have been exemplified for one diagonally bridged derivative, suggesting a photoinduced electron transfer process as fluorescence quenching mechanism for APBIs. From these investigations, guidelines toward highly fluorescent APBI dyes in polar media could be derived.

Keywords: dyes/pigments · dynamic properties · fluorescence · optical properties · perylene bisimide

Introduction

The synthesis of perylene bisimides bearing four aryloxy substituents at the bay area (1,6,7,12 positions) was described for the first time in 1987 by BASF scientists and these dyes were initially applied as an industrial colorant, for example, in foils for plant growth applications which collect solar light.[1] Owing to their outstanding optical and electrochemical properties as well as their remarkable stability against environmental influences,[2] aryloxy-substituted perylene bisimides (APBIs) have been further used as laser dyes[3] and as chromophores for single molecule spectroscopy.[4] Further applications of APBIs have been demonstrated as red emitters for organic and polymeric light-emitting devices (OLEDs and PLEDs).[5] The scope of introducing functional groups at two orthogonal positions (imide and bay positions) has enabled the synthesis of highly functional derivatives and the construction of complex architectures such as rotaxanes,[6] metallosupramolecular squares,[7] rectangles[8] and polymers[9] by self-assembly of APBIs, whilst the introduction of hydrogen-bonding motifs has been utilized for the design of fluorescent organogels[10] based on APBIs. Multichromophore arrays have been designed by combining APBIs either with other perylene bisimides,[11] or different chromophores,[12] in particular, oligo(phenylenevinylene)s,[13] porphyrins,[14] pyrenes,[15] and fullerenes.[16] In such multichromphore systems efficient energy and electron

[a] P. Osswald, Prof. Dr. F. Würthner
Universität Würzburg, Institut für Organische Chemie
Am Hubland, 97074 Würzburg (Germany)
Fax: (+49) 931-888-4756
E-mail: wuerthner@chemie.uni-wuerzburg.de

Supporting information for this article is available on the WWW under http://www.chemeurj.org/ or from the author: Additional graphical materials, details for the determination of transition dipole moments for **4** and macrocycles **5a–d**, optimized geometries of diagonally bridged isomers **5a–d**, temperature-dependent NMR spectra of **6a–c** and ^{1}H NMR spectra of **5a–d** and **6a–d**.

transfer processes were demonstrated, thus they may serve as artificial light-harvesting systems and show good prospects for application in solar cell devices. Water-soluble APBIs are accessible, which exhibit high fluorescent quantum yields in aqueous solution and can be used for cell staining experiments and for the investigation of their interaction with DNA.[17] Furthermore, APBIs were used as fluorescence sensors for fluoride anions.[18]

Despite this remarkable versatility of aryloxy-substituted perylene bisimides, the effect of different conformations on the optical properties of this important class of fluorophores has been barely explored. Single molecule spectroscopic studies revealed that different conformations which originate from the twist of the perylene bisimide chromophore and the orientation of the aryloxy groups have a profound effect on the photophysical properties of *immobilized* APBIs.[19] It was shown in the solid-state structure of a phenoxy-substituted diazadibenzoperylene that the aryloxy groups are oriented in the plane of the perylene bisimide unit,[20] whereas quantum chemical calculations suggested another conformation where the aryloxy units are orientated perpendicular to the perylene core.[19] But also other conformations of the aryloxy residues seem to be easily accessible within a small energy range.[2c,19] Different conformations of the aryloxy residues might have a significant influence on the optical and electrical properties of these dyes by both inductive and mesomeric effects as it has recently been reported that, especially, the optical properties of perylene bisimides are sensitive to the type of bay substituents.[2a,11a,21]

To elucidate the conformational effects on the optical properties of APBI chromophores, conformationally restricted macrocyclic systems which are diagonally bridged through 1,7- and 6,12-linkage (see below, **A**) or laterally bridged (**B**) through 1,12- and 6,7-linkage are properly suited because the conformational freedom of the perylene core should be restricted in these macrocyclic systems and a particular conformation of the aryloxy substituents can be achieved through variation of the length of the bridging unit. Furthermore, in diagonally bridged macrocycles an interconversion of the twisted conformers (*P* and *M* enantiomer) would not be possible without a bond cleavage for shorter bridges. Oligoethylene glycols are appropriate as the bridging units because, on the one hand, this functionality can be introduced in perylene bisimide by etherification of the resorcinol groups at the bay position and, on the other hand, the chain length can be varied through proper choice of ditosylates.

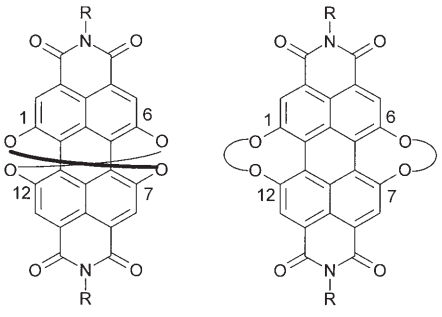

A **B**

Here, we report in detail the synthesis of diagonally bridged macrocyclic perylene bisimides **5a–d** and the corresponding laterally bridged isomers **6a–d**, and the optical and electrochemical properties of these macrocyclic derivatives in comparison to those of the open-chain reference compound **4**.[22] These in-depth investigations clearly reveal the conformational effects of aryloxy bay substituents on the optical as well as electrochemical properties of perylene bisimides. Additionally, the dynamic properties of laterally bridged macrocycles **6a–d** have been studied to gain a deeper inside into the conformational properties of APBIs.

Results and Discussion

Synthesis of macrocyclic perylene bisimides: The syntheses of the open-chain reference compound **4** and the macrocyclic perylene bisimides **5a–d** and **6a–d** are outlined in Scheme 1. Perylene bisimides **1–3** were prepared according to literature.[23]

As an open-chain analogue to the macrocyclic APBIs, **4** was synthesized by etherification of *N*,*N*′-bis(2,6-diisopropylphenyl)-1,6,7,12-tetrakis(3-hydroxyphenoxy)perylene −3,4:9,10-tetracarboxylic acid bisimide (**3**) with 2-(2-[2-(methoxy)ethoxy]ethoxy)ethanol toluene sulfonate (tosylate) and cesium carbonate in DMSO at 80 °C. The triethylene glycol spacer was chosen in order to guarantee the comparability to the macrocyclic compounds. After purification by silica gel column chromatography with ethyl acetate (gradient 5% methanol) as eluent, the ether derivate **4** was obtained in 28% isolated yield. The macrocyclic perylene bisimides **5a–d** and **6a–d** were obtained from perylene bisimide **3** by Williamson's ether synthesis, a reaction which is frequently applied for the synthesis of macrocyclic compounds.[24] For this purpose, a 10^{-3} M solution of **3** in DMSO was treated at 100 °C with the respective oligoethylene glycol ditosylates and cesium carbonate, the latter being known to facilitate the formation of macrocycles.[25] After purification by column chromatography, the diagonally bridged macrocyclic perylene bisimides **5a–d** were isolated in 1–7% yield and, additionally, the laterally bridged isomers **6a–d** (Scheme 1) were obtained for each chain length in 5–15% yield. The overall yield of macrocyclic compounds obtained upon cyclization with diethylene glycol ditosylate (sum of isomers **5b** and **6b**) is 22% which is about 79% of the yield obtained for the open-chain compound **4** (28%) synthesized under similar conditions. This reveals an effective formation of the macrocycles, although the isolated yield of each individual macrocycle was only moderate.

A significantly higher yield was obtained for the laterally bridged isomers compared with those of the diagonally bridged isomers with identical chain length. As the formation of diagonally bridged (**5a–d**) and laterally bridged macrocycles (**6a–d**) occurs from different conformations of the

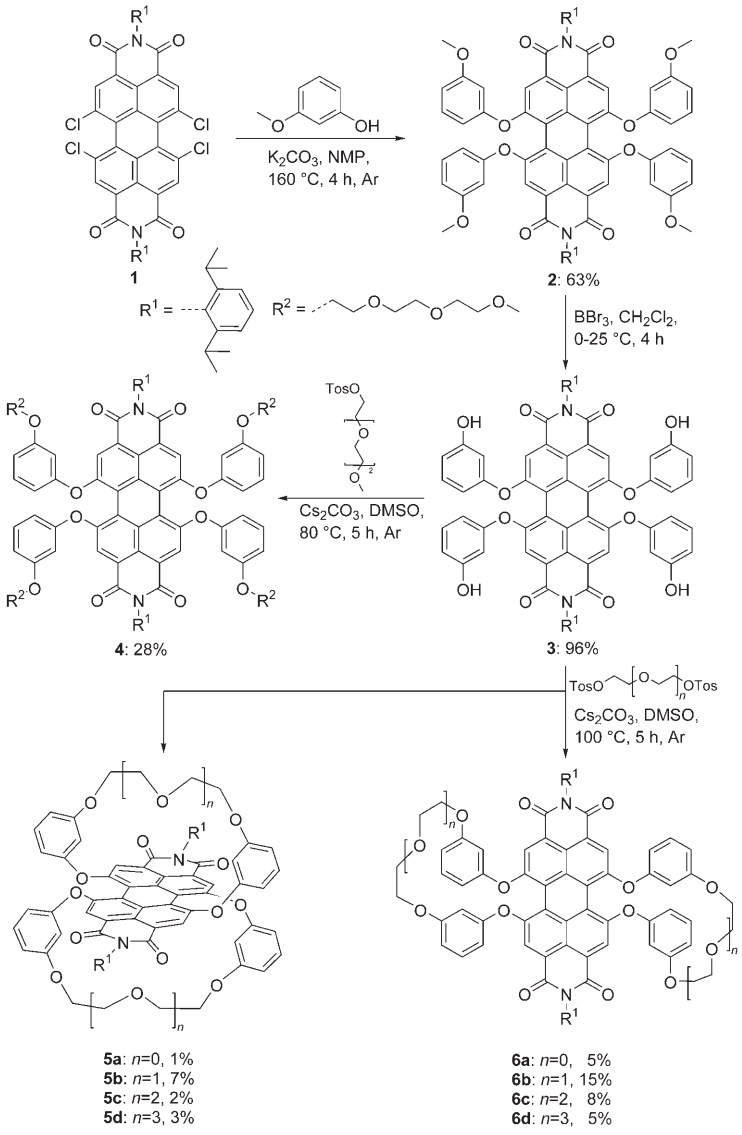

Scheme 1. Synthesis of macrocyclic perylene bisimides.

determined by the entropy of the transition state of the cyclization reaction which becomes unfavorable with increasing chain length.[26]

It is expected that the atropo-enantiomers (*P* and *M*) of diagonally bridged isomers **5a–d** could be resolved by chiral HPLC because an interconversion of the enantiomers of these macrocycles should not be possible. Unfortunately, all attempts to resolve the atropo-enantiomers were unsuccessful. The macrocyclic perylene bisimides **5a–d** and **6a–d** were characterized by ^{1}H NMR spectroscopy and mass spectrometry, and two derivatives (**5b** and **6a**) were characterized by X-ray crystallography.[22]

Structural properties of macrocyclic perylene bisimides: The presence of four resorcinol units in the precursor bisimide **3** may lead to the formation of several isomeric bis(macrocycles) on etherification with oligoethylene glycol ditosylates. The structures of possible isomers are shown in Figure 1. A

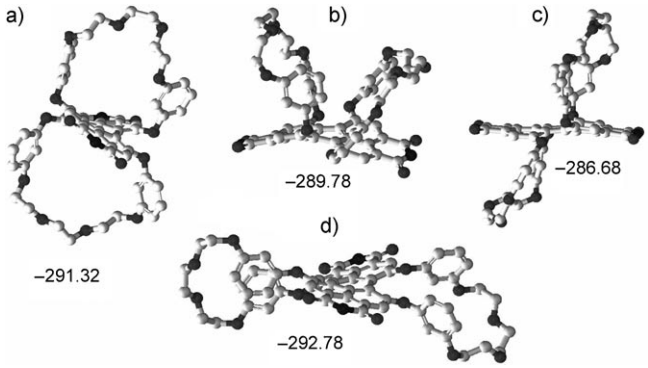

Figure 1. Structures of possible isomeric bis(macrocycles). The structures of the diagonally bridged isomer (a), the two possible straightly bridged isomers (b, c; 1,6- and 7,12-linkage), and the laterally bridged isomer (d) were calculated for triethylene glycol as bridging unit and were optimized by the semi-empirical AM1 method (CaChe Quantum CaChe Workspace 5.0). The heats of formation in kcal mol^{-1} obtained by AM1 calculations are given below the corresponding structure. Hydrogen atoms and the 2,6-diisopropylphenyl imide substituents were omitted for simplicity.

aryloxy residues relative to the perylene core (perpendicular conformation for **5a–d** and horizontal conformation for **6a–d**, see below) in the precursor **3**, the observed difference in yields of isomers **5a–d** and **6a–d** can be attributed to the different free energies of the respective conformations in solution. Thus, the differing yields for regioisomeric macrocycles with identical chain length suggest that the conformations of the aryloxy residues necessary for the formation of the lateral isomers **6a–d** are of lower energy in solution than those required for the diagonally bridged isomers **5a–d**. Furthermore, the isolated yields are dependent on the chain length of the bridging unit and, in turn, on the size of the macrocycle. The diethylene glycol derivatives **5b** and **6b** display the highest yields in each series of isomeric macrocycles. The lower yields of the monoethylene glycol derivatives **5a** and **6a** can be explained by an increased strain present in these macrocycles, whereas the yields of all other derivatives are reliable assignment of the isolated macrocycles to a particular isomer can be achieved by ^{1}H NMR spectroscopy in combination with the previously reported X-ray crystallographic data.[22] Based on these techniques we could conclude[22] that only the two energetically most favorable isomers, that is, a) and d) in Figure 1, were formed in the macrocyclization reaction.

For the structural assignment of the isomers, the resonance of the proton situated between the two oxygen atoms of the resorcin residue is particularly informative because this proton is differently shielded by the aromatic ring current in lateral and diagonal isomers. In comparison to open-chain reference compound **4**, a typical high field shift of this proton (Figure 2, marked resonances) from 6.53 (**4**) to 5.27 ppm for **5a** was observed for the diagonally bridged isomers **5a–d**. Upon increasing the length of the oligoethylene glycol bridge, these resonances were shifted continuously

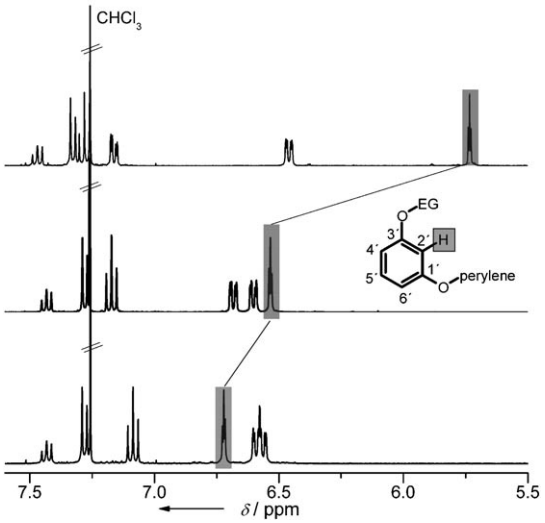

Figure 2. Sections of the ^{1}H NMR spectra (400 MHz) in $CDCl_3$ of the reference compound **4** (middle), **5b** (top), and **6b** (bottom) showing the shift of the proton situated between the two oxygen atoms of the aryloxy substituents (gray). The resonances of the aryloxy residue are displayed.

downfield up to 6.20 ppm for **5d** in the series of diagonally bridged macrocycles.

The shift of this resonance (marked proton H2′) to a higher field is caused by a change of the orientation of the aryloxy residues relative to the perylene core. Because the ring current of the perylene bisimide is responsible for this observation, the shift of these resonances within the series of diagonally bridged isomers can be attributed to an increasing perpendicular orientation of the aryloxy residues relative to the perylene core upon shortening of the oligoethylene glycol chain (see Figure S1 in the Supporting Information). Such a perpendicular orientation was already demonstrated in the solid state structure of **5b**.[22] In contrast, for the lateral isomers **6a–d**, a slight shift of the same proton to lower field from 6.53 ppm (**4**) to 6.70 ppm (**6b–d**) was observed, which is caused by more horizontal orientation of the aryloxy residue relative to the perylene core in comparison to open-chain APBI **4**. This implies that the structural features of the laterally bridged isomers **6a–d** are closely related to those of open-chain perylene bisimides such as **4** in solution. Additionally, the laterally and diagonally bridged isomers could be distinguished by the chemical shift of the bridging ethylene glycol unit. The most pronounced effect was observed for **5a** and **6a**. The ethylene glycol proton resonances of **5a** appeared at δ 3.48 and 3.69 ppm, whereas those of **6a** are located at 4.49 ppm. The shift to higher fields observed for the corresponding resonances of **5a** indicates that the bridging unit is situated in the deshielding area of the perylene core, further confirming the diagonally bridged structure of macrocycles **5**.

Conformational properties of laterally bridged macrocycles 6: As outlined in the previous section, the orientation of the aryloxy substituents is an important structural feature of APBIs which is very distinct for each type of regioisomeric macrocycles. Another characteristic structural feature of APBIs is a twisted conformation of the perylene core resulting in atropo-enantiomers (*P* and *M*) which undergo interconversion. The diagonally bridged **5a–d** and laterally bridged **6a–d** isomers are expected to have different behavior regarding the interconversion process between *P* and *M* enantiomers. In ^{1}H NMR spectra, this can be detected by the diastereotopic methyl resonances of the isopropyl groups present in imide substituents. These resonances are sensitive to chirality present in the molecule and show diagnostic shapes for different stages of the interconversion process. The resonances of these methyl groups for open-chain APBI **4**, and diagonal and lateral isomer **5b** and **6b**, respectively, in ^{1}H NMR spectra in $CDCl_3$ are shown in Figure 3.

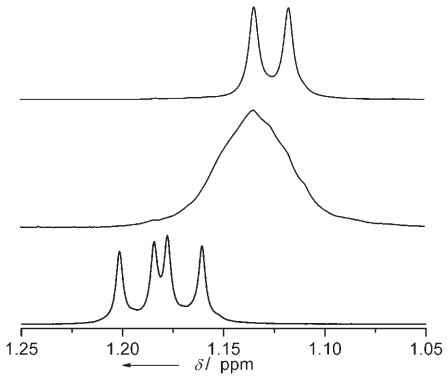

Figure 3. Sections of the ^{1}H NMR spectra (400.13 MHz) of **4** (top), **5b** (bottom), and **6b** (middle) in $CDCl_3$ at 300 K showing the resonances of the diastereotopic methyl groups of the isopropyl units in imide substituents.

For open-chain reference compound **4**, one doublet was observed for these protons (Figure 3, top). The occurrence of one doublet for the methyl groups of isopropyl substituents is explained by a fast interconversion between the atropo-enantiomers ($M \rightleftarrows P$), implying that this interconversion is faster than the proton spin relaxation ("NMR time scale") and the atropo-enantiomers cannot be distinguished by NMR spectroscopy. In contrast, for diagonally bridged macrocycles like **5b** two doublets were observed at room temperature (Figure 3, bottom). This represents the region, where the interconversion process is significantly slower than the spin relaxation, and thus the two atropo-enantiomers can be monitored by the occurrence of two doublets. This corroborates the prediction that an interconversion for this type of isomers should not be possible without a bond cleavage. For the laterally bridged isomers **6b–d**, a broad singlet was observed at room temperature (Figure 3, middle), revealing that the proton spin relaxation occurs at the same time scale as the racemization process (coalescence region). This demonstrates that an interconversion between the enantiomers (*P* and *M*) of laterally bridged isomers **6a–d** is indeed possible.

The dynamic properties of the laterally bridged macrocyclic perylene bisimides **6a–d** were investigated in detail by

temperature-dependent ^{1}H NMR spectroscopy. The protons of the diastereotopic methyl groups of isopropyl units in the imide positions of the perylene bisimide are properly suited to monitor the interconversion process. The measurements for the laterally bridged macrocycles **6a–d** were performed in $CDCl_3$ or [D_2]tetrachloroethane and additionally the interconversion process of open-chain APBI **2** was investigated in $CDCl_3$ for the purpose of comparison and validation of the experimental setup. The data were evaluated according to the coalescence method [Eqs. (1) and (2)].[27]

$$k_c = \frac{\pi}{\sqrt{2}}|\Delta\nu| \quad (1)$$

$$\Delta G^{\neq} = R \cdot T_c \cdot \ln\left(\frac{R \cdot T_c}{k_c \cdot N_A \cdot h}\right) \quad (2)$$

In Figure 4, the temperature-dependent changes of the methyl resonances of lateral isomer **6d** are shown exemplarily and for the remaining compounds **6a–c**, the spectra are given in Figures S11 and S12, Supporting Information. As can be seen in Figure 4, one doublet was observed at high temperatures (above 304 K), revealing a fast equilibrium between the conformational enantiomers on the NMR time scale as observed for the open-chain APBI **4** at 298 K. Upon cooling the sample, broadening of the signal occurred and below 280 K two doublets arose which can be attributed to a slow interconversion between the two core-twisted enantiomers (*P* and *M*). From line broadening, a coalescence temperature of 292 K was determined for **6d** and the difference in chemical shift of the two enantiomers (*P* and *M*) $\Delta\nu$ at lower temperature (253 K) resulted to 19.9 Hz. According to Equations (1) and (2), the free activation enthalpy $\Delta G^{\neq}$ for the interconversion process of **6c** was estimated to 63 kJ mol^{-1} at 292 K. For **2** and **6a–c**, the free activation enthalpies for the interconversion $\Delta G^{\neq}$ were estimated analogously and the obtained values are given in Table 1.

Table 1. Activation parameters for the interconversion of atropo-enantiomers of laterally bridged macrocycles **6** and open-chain APBI **2** determined by temperature-dependent ^{1}H NMR spectroscopy.

	Solvent	$\Delta\nu$ [Hz]	T_c [K]	$\Delta G^{\neq}_{T_c}$ [kJ mol^{-1}]
6a	Cl_2DC-$CDCl_2$	26.6	347	74 ± 3
6b	$CDCl_3$	23.6	301	64 ± 3
6c	$CDCl_3$	19.9	295	63 ± 3
6d	$CDCl_3$	19.9	292	63 ± 3
2	$CDCl_3$	6.3	271	60 ± 3

Within the series of laterally bridged macrocycles **6a–d**, the activation parameters clearly correlate with the ring size of the macrocycles. For the large macrocycles **6b–d**, the coalescence temperature and free enthalpy of activation are only scarcely dependent on the chain length (see Table 1). Furthermore, the inversion barriers for macrocycles **6b–d** are only slightly increased compared with that of open-chain APBI **2**, demonstrating similar conformational behavior of

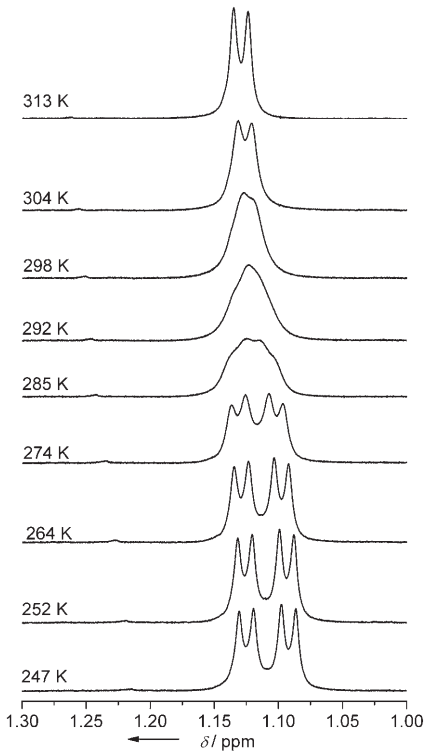

Figure 4. Sections of the temperature-dependent ^{1}H NMR spectra (600 MHz) of **6d** in $CDCl_3$. Displayed are the resonances of the diastereotopic methyl groups of isopropyl units present in imide substituents.

these compounds. In contrast, macrocycle **6a** showed a higher coalescence temperature (347 K) compared with the other laterally bridged macrocycles **6b–d**, hence the inversion barrier is increased to 74 kJ mol^{-1} at 347 K. This trend is in contrast to that observed for 2,2′-substituted biphenyls where the interconversion barriers were shown to increase with increasing chain length of the alkyl bridge.[28] But it has to be noted that the conformational restriction imposed by ethylene glycol chains is smaller than that of the corresponding alkyl chains owing to the higher flexibility resulting from the presence of oxygen atoms. Nevertheless, the trend observed for macrocyclic perylene bisimides **6a–d** highlights the importance of conformational changes of the aryloxy residues for the *M*⇄*P* interconversion process of APBIs. Especially for **6a**, the movement of the aryloxy residues is strongly restricted by the presence of a short bridging unit.

The large energy difference between the ground and the transition state of the racemization process revealed by the free activation enthalpy of **2** implies that the population of the transition state is negligible at room temperature. To gain a deeper insight into the interconversion process of APBIs, calculations were performed using MM2 force field which has been widely applied for such purpose.[13b,29] Thus, the heats of formation were calculated for the open-chain APBI **2** with perpendicular orientation of the aryloxy groups in dependence on the twist angle of the perylene core. The calculations were performed for different dihedral

angles θ of the central six-membered ring of the perylene core in the range of -75 to 0° (M enantiomer) and the obtained results were mirrored to gain the heats of formation for the opposite enantiomer (P enantiomer, $\theta = 0$–75°). This is justified because enantiomers are considered and no other structural differences, except the opposite twist, have to be taken into account. The twist angle dependent distribution of the obtained energies (heat of formation) relative to the local minimum is shown in Figure 5, top. The local minimum is reached at a twist angle of 28°, which is in good agreement with that observed for a structurally related diazadibenzoperylene derivative[20] and **6a** in the solid state.[22]

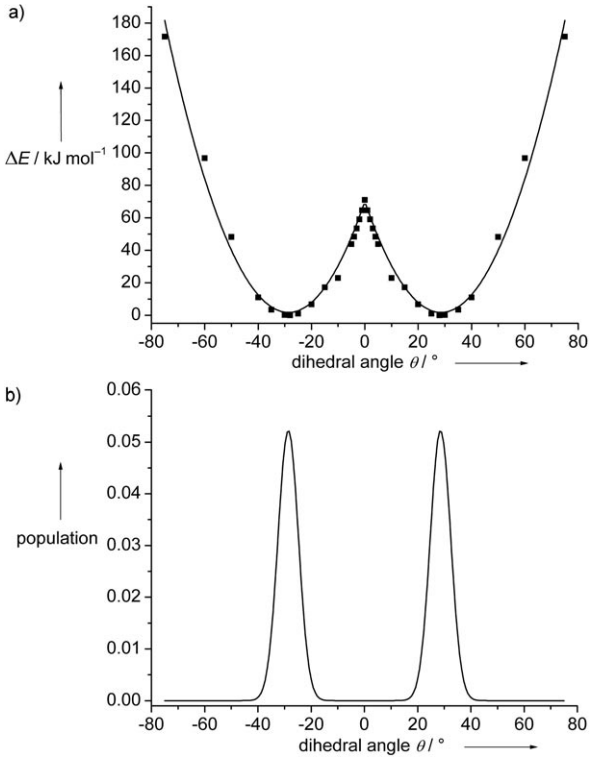

Figure 5. Calculated energy distribution (top) and resulting normalized population of conformations with different dihedral angles θ (bottom) of **2** at 293 K obtained by MM2 force field calculation.

From these calculations, the energy barrier for the interconversion of **2** was obtained according to Equation (3) and resulted to 66 kJ mol^{-1} which is in proper agreement with that obtained experimentally by NMR spectroscopy (60 kJ mol^{-1}).

$$\Delta H_{rot} = \Delta H_f\ (\theta = 0^\circ) - \Delta H_f\ (\theta = 28^\circ) \qquad (3)$$

The slight difference between the theoretical and experimental values can be explained in terms of the unknown structure of the transition state and by the fact that the activation enthalpy ΔH is estimated by molecular modeling in the gas phase, while the free enthalpy of activation $\Delta G^{\neq}$ was obtained by NMR experiments in solution. From the dependence of the heat of formation on the dihedral angle θ, the population of conformations exhibiting different twist angles was calculated according to Boltzmann statistic (see Experimental Section). The normalized population of conformations with different twist angles at 293 K is shown in Figure 5, bottom. The proper match of the calculated values with that determined by NMR spectroscopy confirms that APBIs possess a rather defined twist angle (28°) and reveals a negligible population of angles $\theta < 15°$ for APBIs in solution.

Electrochemical properties of macrocyclic perylene bisimides: Open-chain APBIs such as **4** display two reversible reduction waves and one reversible oxidation wave within the potential range from -1.50 to $+1.15$ V versus the ferrocene/ferrocenium couple. In order to investigate the influence of different conformations of the aryloxy substituents on the electrochemical properties of APBIs, the redox potentials of macrocycles **5a–d** and **6a–d** were determined by cyclic voltammetry in dichloromethane using tetrabutylammonium hexafluorophosphate (TBAHFP) as supporting electrolyte. All half-wave potentials are referred to the redox couple of ferrocence/ferrocenium as internal standard. The first and the second reduction half-wave potentials as well as the oxidation potentials of macrocyclic perylene bisimides **5a–d** and **6a–d** are collected in Table 2, and the cyclic

Table 2. Redox potentials (in V) of macrocycles **5a–d** and **6a–d**, and reference compound **4** in dichloromethane (0.1 M TBAHFP) versus ferrocene/ferrocenium as internal reference.[a]

	$E_{1/2}$ (PBI$^-$/PBI^{2-})	$E_{1/2}$ (PBI/PBI$^-$)	$E_{1/2}$ (PBI/PBI$^+$)
5a	−1.30	−0.97	>1.17
5b	−1.38[b]	−1.07	1.16[b]
5c	−1.39	−1.12	1.09[b]
5d	−1.39	−1.17	0.98
6a	−1.32	−1.07	1.05
6b	−1.30	−1.11	0.91
6c	−1.35	−1.14	0.90
6d	−1.36	−1.14	0.90
4	−1.35	−1.14	0.91

[a] Determined from the reversible redox process with $\Delta E \approx 60$–100 mV between the oxidative and reductive peak maxima, error ± 0.05 V. [b] Quasi-reversible.

voltammograms of **5c** and **6c** are exemplified in Figure 6. Macrocycles **5a–d** and **6a–d** showed two reversible reduction waves which is typical for APBIs. Whilst for the macrocycles **5d** and **6a–d** nicely resolved reversible oxidation waves are observed between 0.9 and 1.05 V, the oxidation of diagonal isomers **5a–c** occur at higher potentials and are obscured by an irreversible process.

For the laterally bridged macrocycles **6b–d**, the determined half-wave potentials for the reduction and oxidation processes are similar to those of open-chain APBI **4**. Only the smallest macrocycle **6a** bearing monoethylene glycol bridges exhibits a higher oxidation potential (1.05 V) compared with that of **4** and **6b–d** (around 0.90 V), whereas the

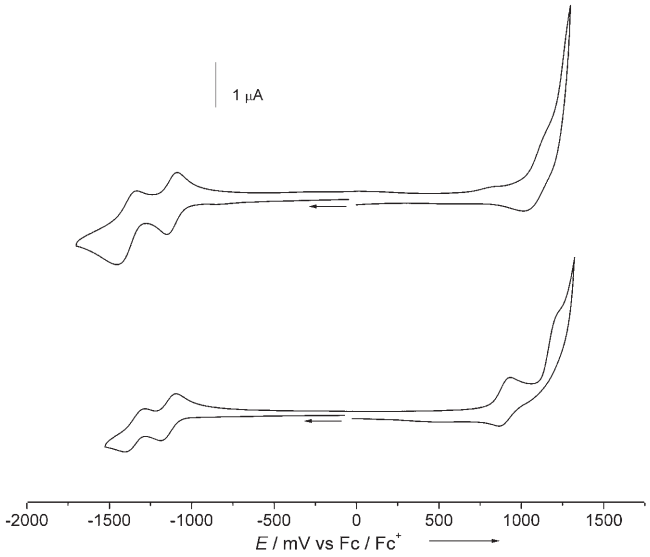

Figure 6. Cyclic voltammograms of **5c** (above) and **6c** (below) in dichloromethane (0.1 M TBAHFP, sweep rate 100 mV s^{-1}).

reduction potentials at −1.07 and −1.32 V are similar to those obtained for **6b–d** (Table 2). The comparatively high oxidation potential for **6a** can be explained in terms of the conformational restriction imposed by the shorter bridging unit.

The observed reduction potentials for diagonally bridged macrocycles **5c**,**d** with longer bridges are pretty close to that observed for the open-chain reference compound **4**, whilst for the derivatives **5a**,**b** with shorter bridges an increase of the reduction potential with decreasing chain length was observed. For macrocycle **5a**, a reduction potential of −0.97 V was determined that is almost 0.2 V higher than that of macrocycle **5d** (−1.17 V). Furthermore, the conformational properties of the aryloxy substituents have a pronounced influence on the respective oxidation potentials of diagonally bridged macrocycles, as the oxidation potentials were found to increase from 0.98 (**5d**) to 1.16 V (**5b**) with decreasing chain length of the macrocycles (Table 2). For **5a**, no oxidation wave of the perylene bisimide could be observed in the available scanning range due to irreversible oxidation at >1.17 V. The significant changes of the redox potentials observed in the series of macrocyclic perylene bisimides **5a–d** reveal that different conformations of the aryloxy substituents, that is, the orientation of the aryloxy residue relative to the perylene core, have an appreciable effect on the redox properties of APBIs.

Optical properties of macrocyclic perylene bisimides: The optical properties of the macrocyclic perylene bisimides were investigated by UV/Vis and fluorescence (steady-state and time resolved) spectroscopy. In Figure 7, the absorption spectra of macrocycles **5a–d** and **6a**,**c**,**d** are shown in comparison to that of open-chain reference **4** (the spectrum of **6b** is almost identical with that of **6c**, thus it is not depicted). The absorption spectra of laterally bridged macrocycles

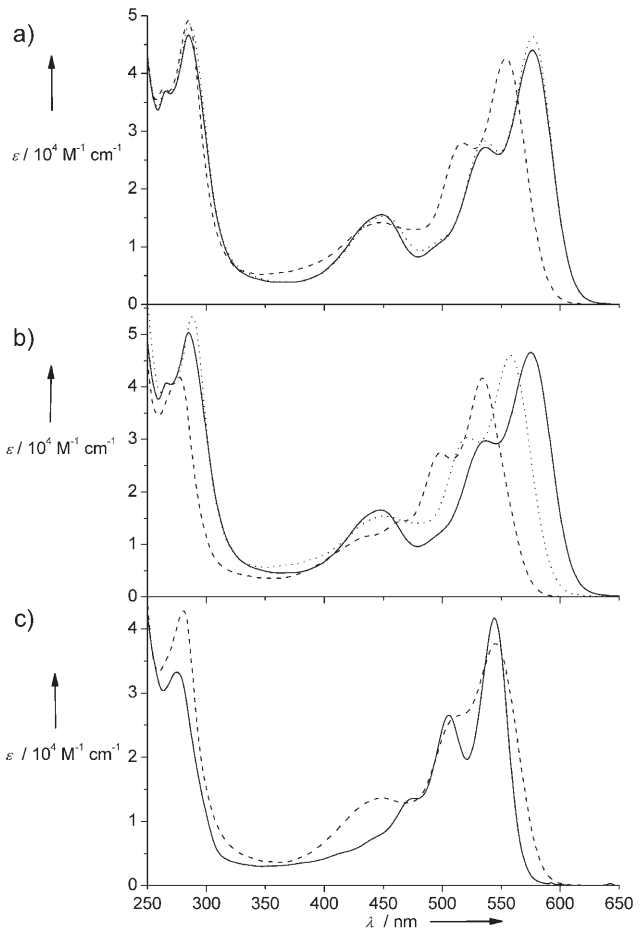

Figure 7. UV/Vis absorption spectra in dichloromethane: a) Laterally bridged macrocycles **6a** (-----), **6c** (•••••), and **6d** (——); b) diagonal isomers **5b** (-----) and **5d** (•••••) in comparison to reference compound **4** (——); c) diagonal isomers **5a** (——) and **5c** (-----).

6a–d (Figure 7a) are typical for APBIs with a maximum around 580 nm assigned to the S_0–S_1 transition, a shoulder of the second vibronic progression and a broad maximum at 450 nm related to the S_0–S_2 transition. For the derivatives **6b–d**, the absorption maxima as well as the molar absorption coefficients are almost identical to those of open-chain reference compound **4** (see Figure 7b); therefore, the latter may possess a similar conformation to that of laterally bridged isomers **6a–d** (Figure 7a).

Macrocycle **6a** with the smallest bridging unit adopts an exceptional position among the lateral isomers because the maximum of the S_0–S_1 transition is hypsochromically shifted by 20 nm compared with that of **6b–d** and a decrease of the molar absorption coefficient is observed. The exceptional behavior of **6a** was already demonstrated before by cyclic voltammetry (higher oxidation potential compared to **6b–d**, see Table 2), and also by NMR spectroscopy as the interconversion barrier for this compound (T_c = 347 K) is significantly higher compared to those of other derivatives (T_c = 295 K). Therefore, the observed differences in the absorption properties between **6a** and **6b–d** are presumably due to

the conformational restriction in **6a** imposed by the short bridging unit.

For the diagonally bridged isomers **5a–d**, much more pronounced spectral differences are observed in comparison to open-chain reference compound **4** (Figure 7b,c). The absorption maxima related to the S_0–S_1 transition for diagonally bridged macrocycles **5a–d** are shifted up to 41 nm (**5b**) towards shorter wavelength from 575 (**4**) to 558 (**5d**), and 545 (**5a**,**c**), and 534 nm (**5b**). This hypsochromic shift is further related to the chain length of the bridging unit as the comparison of the absorption maxima of **5b** and **5d** reveals (Figure 7b). Furthermore, a decrease of the absorption coefficient ε is observed for macrocycles **5a–c** in comparison to reference compound **4**. As the transition dipole moments for the S_0–S_1 transition of these diagonally bridged macrocycles **5a–d** (7.6–8.0 Debye) equal that of reference compound **4** (7.8 Debye), this effect can be attributed to spectral broadening and shift of intensity into higher vibronic progressions of the S_0–S_1 transitions (Figure 7c and see Supporting Information for details). The observed hypsochromic shift, on the other hand, may be attributed to the formation of a conformer with less conjugation between the electron-donating aryloxy group and the electron-deficient perylene bisimide core.

The fluorescence properties of reference compound **4** and macrocycles **5a–d** and **6a–d** in dichloromethane are summarized in Table 3 and the normalized fluorescence spectra are shown in Figure 8 (see also Figure S2, Supporting Information). As can be seen from Table 3, the fluorescence quantum yields and lifetimes of the lateral isomers **6a–d** are almost indistinguishable with that of the open-chain reference compound **4**, which again indicates that the behavior of these isomers is similar to that of the open-chain APBI derivatives.

In contrast to the lateral isomers **6a–d**, for which almost identical fluorescence quantum yields were observed, the fluorescence quantum yields of diagonally bridged macrocycles **5a–d** are tremendously decreased from 0.90 for **5d** to <0.02 for **5a** (Table 3, 4th column). This effect can be attributed to an increase of the non-radiative rate constants k_{nr} (**4** $\approx$ **5d** $<$ **5c** $<$ **5b** $<$ **5a**), whereas the radiative rate constants k_r are similar for all compounds presented here.

To shed more light on the excited state properties of diagonally bridged macrocyclic perylene bisimides, UV/Vis and fluorescence spectroscopy (steady-state and time resolved) were carried out for diagonal isomer **5b** and reference compound **4** in solvents of different polarity (Table 4, for spectra see Figure S3, Supporting Information).

As can be seen from the data in Table 4, the spectral position of the absorption as well as the emission maxima of **5b** are only slightly dependent on the solvent polarity. The observed negligible solvatochromism indicates the apolar character of the ground and excited state of **5b**. Furthermore,

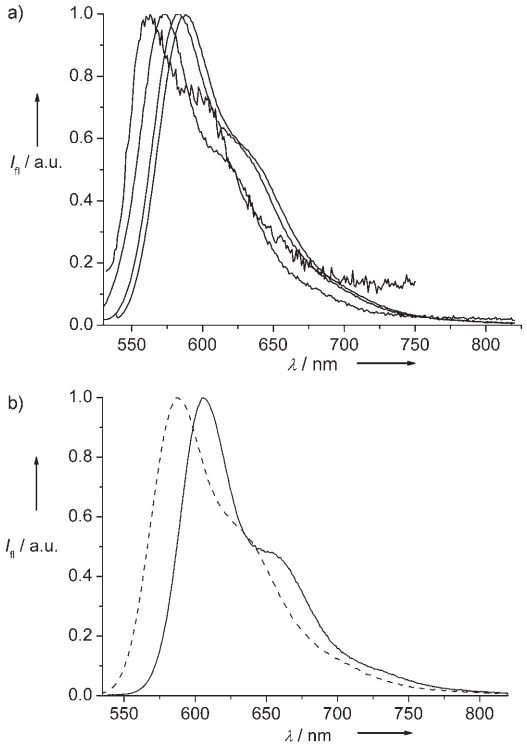

Figure 8. Normalized fluorescence spectra in dichloromethane of diagonally bridged isomers (above) **5a–d** (left to right) and lateral isomers (below) **6a** (-----) and **6d** (——).

Table 3. Emission properties of macrocyclic perylene bisimides in dichloromethane.

	λ_{max} [nm]	$\Delta\lambda$ [nm][a]	Φ_{fl}[b]	τ_{fl} [ns][c]	k_r [s^{-1}][d]	k_{nr} [s^{-1}][e]
4	609	34	0.89	5.6	1.7×10^8	2.0×10^7
5a	562	18	<0.02	<0.5	$>4.0\times10^7$	$>2.0\times10^9$
5b	573	39	0.09	0.8	1.1×10^8	1.1×10^9
5c	582	37	0.43	2.7	1.6×10^8	2.1×10^8
5d	588	30	0.90	5.5	1.6×10^8	1.8×10^7
6a	588	34	0.78	5.4	1.4×10^8	4.1×10^7
6b	605	28	0.82	5.3	1.6×10^8	3.4×10^7
6c	606	24	0.84	5.6	1.5×10^8	2.9×10^7
6d	606	29	0.82	5.5	1.5×10^8	3.6×10^7

[a] The Stokes shift $\Delta\lambda$ was calculated as the difference in absorption and emission maximum. [b] $\Phi_{fl}\pm0.03$. [c] $\tau_{fl}\pm0.2$. [d] $k_r = \Phi_{fl}\cdot\tau_{fl}^{-1}$. [e] $k_{nr} = (1-\Phi_{fl})\cdot\tau_{fl}^{-1}$.

Table 4. Solvent-dependent absorption and fluorescence properties of **5b**.

Solvent	λ_{abs} [nm]	λ_{em} [nm]	Φ_{fl}[a]	τ_{fl} [ns][b]	k_r [s^{-1}][c]	k_{nr} [s^{-1}][d]
dimethylsulfoxide	553	590	<0.02	<0.7	$>2.9\times10^8$	$>1.4\times10^9$
dichloromethane	534	573	0.09	0.8	1.1×10^8	1.1×10^9
THF	545	571, (613)[e]	0.14	1.2	1.2×10^8	7.1×10^8
diethyl ether	543	568, (611)[e]	0.98	5.6	1.8×10^8	3.6×10^6
toluene	548	569, (614)[e]	0.95	5.4	1.8×10^8	9.3×10^6

[a] $\Phi_{fl}\pm0.03$. [b] $\tau_{fl}\pm0.5$. [c] $k_r = \Phi_{fl}\cdot\tau_{fl}^{-1}$. [d] $k_{nr} = (1-\Phi_{fl})\cdot\tau_{fl}^{-1}$. [e] Vibronic progression.

the shape of the absorption spectrum is similar for all solvents investigated, implying no significant conformational changes for **5b**.

The fluorescence intensity of **5b**, on the other hand, is strongly dependent on the polarity of the solvent (see Table 4, 4th column). In polar solvents such as DMSO, diagonally bridged macrocycle **5b** is almost non-fluorescent ($\Phi_{fl} \approx 0$). In the medium polar solvents dichloromethane and THF ($\varepsilon_r = 8.9$ and 7.4, respectively) the fluorescence quantum yields remain low (0.09 and 0.14, respectively). However, in solvents of low polarity such as diethyl ether or toluene ($\varepsilon_r = 4.3$ and $\varepsilon_r = 2.3$, respectively), **5b** exhibits a fluorescence quantum yield of nearly unity ($\Phi_{fl} = 0.98$ and 0.95). Also the fluorescence lifetime increased to 5.6 ns and 5.4 ns in diethyl ether and toluene, respectively, compared with DMSO ($\tau_{fl} < 0.7$ ns), and these values match well with that determined for the open-chain reference compound **4** (5.6 ns) in dichloromethane and other APBIs (5.9–7.4 ns).[3,4d,6,9a,19,30] The observed relationship between the fluorescence quantum yield of **5b** and the polarity of the solvent indicates fluorescence quenching by a competitive charge transfer process (see Figure S4, Supporting Information).[31]

The fluorescence properties of **4**, which comprises different orientation of the aryloxy residues as outlined before, are solvent dependent as well. The fluorescence quantum yields of **4** in polar solvents are low with 0.06 and 0.14 in methanol and acetonitrile, respectively, and increased continuously in dependence on the solvent polarity to 0.21 (ethanol) and 0.40 (1-butanol). In comparison to **5b**, high fluorescence quantum yields (0.75–0.84) were observed already in medium polar solvents such as ethyl acetate or dichloromethane and remained constant (≈ 0.85) in solvents of lower polarity (Figure S4, Supporting Information).

Discussion of the optical and electrochemical properties of 5 and 6: In order to explain the observed largely differing optical properties of these APBIs, the optical band gaps and the frontier orbitals of macrocycles **5a–d** and **6a–d** as well as of open-chain APBI **4** were determined. The optical band gap E_{gap}^{OS} was assessed from the cross section of the normalized absorption and emission spectra (Table 5). For the series **5a–d**, the data shown in Table 5 reveal a continuous increase of E_{gap}^{OS} from 2.17 eV (**5d**) to 2.25 eV (**5a**) with decreasing chain length of the bridging unit. The band gaps E_{gap}^{CV} determined from cyclic voltammetry show excellent agreement to those obtained from optical spectroscopy. The remarkable correspondence of the band gaps E_{gap}^{OS} and E_{gap}^{CV} can be explained by the fact that the S_0–S_1 transition in these APBIs is related to an almost pure electronic excitation of an electron from the HOMO to the LUMO. The lateral isomers **6a–d** exhibit ≈ 0.1 eV smaller band gap that show somewhat larger deviations (0.05–0.08 eV) between E_{gap}^{OS} and E_{gap}^{CV}. Again, the value of APBI **4** is in perfect agreement with those of **6a–d**.

The energy of the LUMO was assessed from the first reduction potential by taking into consideration the potential of ferrocene (−4.8 eV) with respect to the zero vacuum level.[5b] Then the energy of the HOMO was calculated by subtracting the determined optical band gap E_{gap}^{OS} from the LUMO energy. As can be seen from Table 5 and Figure 9, a continuous decrease of the energy of the HOMO from −5.8 (**5d**) to −6.1 eV (**5a**) with respect to the zero vacuum level was observed upon shortening the chain length of the macrocycles. In a similar manner, the energy of the LUMO is

Table 5. Optical band gaps determined from optical spectroscopy (OS) and cyclic voltammetry (CV) and calculated HOMO and LUMO levels in eV for diagonally bridged **5a–d** and laterally bridged macrocycles **6a–d** and reference compound **4**.

	E_{gap}^{OS}[a]	E_{gap}^{CV}[b]	LUMO[c]	HOMO[d]
5a	2.25	>2.14[e]	−3.83	−6.08
5b	2.24	2.23	−3.73	−5.97
5c	2.20	2.21	−3.68	−5.88
5d	2.17	2.15	−3.63	−5.80
6a	2.18	2.12	−3.73	−5.91
6b	2.10	2.02	−3.69	−5.79
6c	2.09	2.04	−3.66	−5.75
6d	2.10	2.04	−3.66	−5.76
4	2.10	2.05	−3.66	−5.71

[a] Determined from the intersection of the normalized absorption and emission spectra. [b] Calculated from the difference of oxidation and reduction potentials. [c] Calculated from the first reduction potential and the potential of ferrocene relative to the zero vacuum level. [d] Calculated from E_{gap}^{OS} and the LUMO level. [e] Not accessible due to irreversible oxidation at 1.17 V.

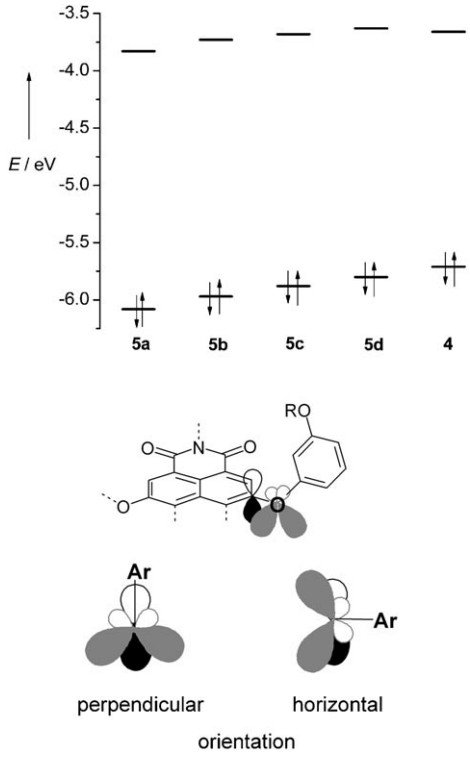

Figure 9. Energies of HOMO and LUMO for diagonally bridged macrocycles **5a–d** and reference compound **4** (above), and schematic representation of the orbital interactions between the perylene core and the aryloxy substituents (below); Ar denotes the 3-alkoxyphenyl residue.

decreased from −3.6 (**5d**) to −3.8 eV (**5a**), although this effect is less pronounced than that observed for the HOMO energies (Figure 9, top). The different energy level of the frontier orbitals corresponds to the increase of the band gap, and thus to the hypsochromic shift of the absorption maximum observed for macrocyclic perylene bisimides **5a–d** (Figure 7). In contrast, the energy of the HOMOs (−3.66 eV) as well as those of the LUMOs (−5.75 eV) remain constant in the series of lateral isomers **6b–d** and resemble those calculated for open-chain reference compound **4** (Table 5).

To explain the conformational impact on the HOMO and the LUMO energies of laterally and diagonally bridged isomers **5a–d** and **6a–d**, the electronic coupling between the PBI core and the aryloxy substituents was elucidated. It can be considered that APBIs are composed of the electron-poor perylene bisimide core and the electron-rich aryloxy substituent and, accordingly, the MO of APBIs must be a result of the interaction of these molecular fragments.

The comparison of the oxidation potentials determined for open-chain APBI **4** ($E_{ox}=+0.91$ V; $E_{red}=-1.14$ V vs Fc/Fc^+) and macrocyclic perylene bisimides **6b–d** ($E_{ox}=+0.90$ V; $E_{red}=-1.14$ V vs Fc/Fc^+) with that of the unsubstituted *N*,*N*′-bis(2,6-diisopropylphenyl)perylene-3,4:9,10-tetracarboxylic acid bisimide ($E_{ox}=+1.29$ V; $E_{red}=-1.01$ V vs Fc/Fc^+)[32] reveals that the HOMO is almost 0.4 eV higher for APBIs, whilst the LUMO level is only raised by about 0.1 eV.

On the other hand, the redox potentials and the related HOMO/LUMO energies of APBIs **4** and **6a–d** are not altered in comparison to other APBIs bearing less electron-rich aryloxy substituents in the bay position (e.g., tetraphenoxy-substituted perylene bisimides: $E_{ox}=+0.89$ V, $E_{red}=-1.10$ V).[5c] This fact suggests that there is no significant conjugation between the perylene bisimide core and the respective aryloxy residue. The absence of conjugative effects between the perylene bisimide core and the aryloxy residues was also pointed out in literature.[5b] This finding strongly suggest that the electron-rich HOMO of APBIs originates from the primordial HOMO of the perylene bisimide core upon conjugation to four oxygen atoms (+M effect) directly attached to the PBI core. In contrast, the LUMO of macrocycles **6b–d** and open-chain reference **4** differ only slightly from that of the unsubstituted perylene bisimide, indicating that the LUMO in APBIs can be ascribed to the primordial perylene bisimide core LUMO.

In order to assess the presence of mesomeric effects between the aryloxy substituent and the perylene core in APBIs, the CO bond lengths of **5b** and **6a**, obtained from X-ray crystallography,[22] were analyzed. The length of the bond connecting the perylene bisimide core and the oxygen atom of the aryloxy residue was determined to 1.375 ± 0.003 Å (**5b**) and 1.372 ± 0.007 Å (**6a**) which is significantly shorter than the length expected for a C_{sp^3}–O single bond (1.440 Å).[33] Furthermore, these values are in good agreement to bond lengths observed for 1,4-dimethoxybenzene (1.360 Å)[34] and 4-nitroanisol (1.351 Å)[35] in the solid state. Thus, the observed partial double bond character for these CO bonds confirms the presence of mesomeric effects between the perylene bisimide core and the oxygen atoms directly attached to the PBI core.[33]

Therefore, we can relate the observed decrease of the HOMO energy from **5d** to **5a** to a decreased conjugation of the electron-donating oxygen atoms and the electron-poor perylene bisimide core. Since both frontier orbitals determine the optical band gap, also the observed hypsochromic shift can be ascribed to a reduced electron donation of the appended aryloxy substituents in the series of diagonally bridged macrocycles **5a–d**.

The pronounced impact of the orientation of the aryloxy residues on the APBI frontier orbitals, however, remains to be explained. Clearly, the mesomeric effect must be associated with the interaction of the lone pairs of the oxygen atoms directly attached to the perylene bisimide core and the perylene bisimide π-system (Figure 9, bottom). As the degree of conjugation is related to the overlap of the participating orbitals, it seems reasonable that the angle of the oxygen lone pair orbitals relative to the π-orbitals of the perylene core determines the magnitude of conjugation. As schematically shown in Figure 9, the overlap of the respective orbitals is most effective for a horizontal orientation of the aryloxy residue (as given in **6a–d**) and less effective for a perpendicular orientation of the aryloxy residue (as given in **5a**,**b**).

Therefore, the electron donation from the aryloxy bay substituents to the PBI core can be directly related to the dihedral angle γ between the aryloxy groups and the perylene bisimide core (see Figure 10). This angle describes the orientation of the aryloxy residues relative to the perylene core and a value of 90° corresponds to a perpendicular orientation, whereas a γ value of 0° relates to a horizontal orientation. The dihedral angle γ was estimated from AM1 calculation as the mean value of the four aryloxy substituents (Figure 10). For the diagonally bridged isomers **5**, an increase of the dihedral angle γ was observed with decreasing ring size of the macrocycle from 48° (**5c**) to 79° (**5a**). Therefore, the conjugation between the aryloxy residue and the perylene core is determined by the orientation of the aryloxy residues. Accordingly, the structural origin of the hypsochromicity is given by the different orientations of the aryloxy residue as schematically shown in Figure 10 (bottom).

Likewise, the relative position of the aryloxy residue to the oxygen lone pairs can be assessed from AM1 calculations by the dihedral angle ω (Figure 10, top). In accordance with the dihedral angle γ, an angle ω of 0° corresponds to the conformation with the largest interaction between the aryl residue and the oxygen atom, whereas a 90° conformation does not possess any conjugation, no matter whether a horizontal ($\gamma=0°$) or perpendicular conformation ($\gamma=90°$) is present. The ω values for diagonally bridged macrocycles **5** increase with increasing ring size from 11° (**5a**) to 54° (**5c**) which reveal an opposite trend in comparison to the dihedral angle γ (Figure 10, top). These results indicate that for the smallest macrocycles **5a**,**b**, the lone pairs of the oxygen

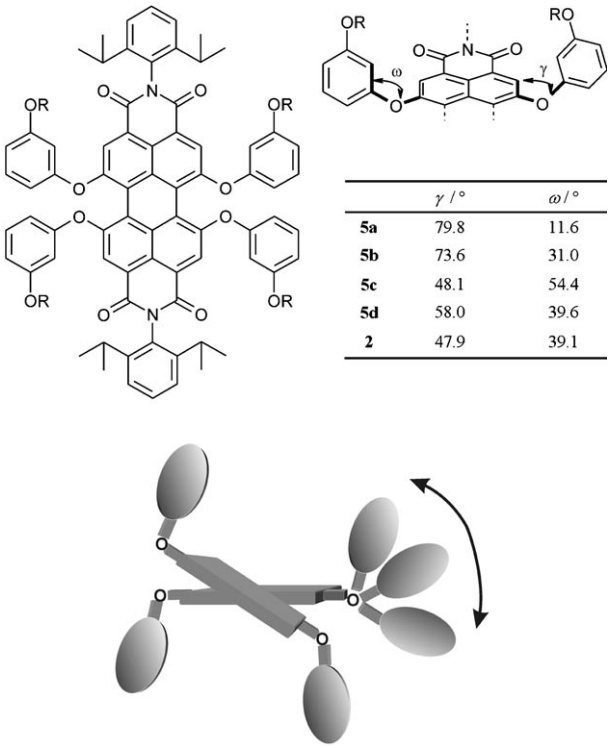

	γ / °	ω / °
5a	79.8	11.6
5b	73.6	31.0
5c	48.1	54.4
5d	58.0	39.6
2	47.9	39.1

Figure 10. Definition and values of the dihedral angles γ and ω for macrocyclic perylene bisimide **5a–d** and open-chain APBI **2** (top) obtained from semiempirical AM1 calculations using Cache Quantum Cache Workspace 5.0. Schematic representation of the possible conformations of the aryloxy residues (bottom). The curved arrow indicates the possible movement of the aryloxy residues.

is conjugated more strongly to the aryloxy residue, whereas for the larger APBIs **5c**,**d**, the oxygen lone pairs are more strongly conjugated to the perylene bisimide core.

The pronounced variation of the fluorescence quantum yield of diagonally bridged macrocycles **5a–d** can now be attributed to the different electronic properties that arise for different dihedral angles γ and ω. On the one hand, Figure 9 reveals the decrease of the HOMO level upon fixation of the aryloxy residue in a perpendicular position by means of short oligoethylene glycol bridge in **5a** (large γ of 80°). On the other hand, the angle ω goes to a minimum (12°) for this compound leading to the most electron-rich resorcin subunit. Indeed, the oxidation potential for 1,3-dimethoxybenzene[36] is 1.08 V versus Fc/Fc^+ which is lower than the oxidation potential of APBIs **5a**,**b**. Thus, it is reasonable to relate the observed fluorescence quenching for **5a**,**b** to a photoinduced electron transfer process from the electron-rich aryloxy group to the electron-poor perylene bisimide core. For **5c** the quenching is less effective but still substantial. For the better conjugated conformations, that is, laterally bridged isomer **6a–d** and the diagonally bridged derivative **5d** with the longest oligoethylene glycol chain, in which the electron-deficient perylene bisimide core and the electron-rich resorcin units experience the strongest electronic coupling (see Figure 9), the radiative decay becomes favorable. Similarly, the solvent-dependent fluorescent properties of APBIs **4** and **5b** (Figure S4, Supporting Information) support a photoinduced electron transfer process as an explanation for the fluorescence quenching in accordance with predictions based on the Rehm–Weller equation.[31] Thus, a photoinduced electron transfer process is a very plausible fluorescence quenching mechanism for APBI.

Conclusion

In summary, the synthesis of macrocyclic perylene bisimides **5a–d** and **6a–d** with different chain lengths was achieved by Williamson's etherification reaction and their structures were elucidated by NMR spectroscopy in combination with X-ray analysis reported previously.[22] Whilst diagonally bridged derivatives **5a–d** exhibit a rigid twisted core, atropoenantiomeric laterally bridged macrocycles **6a–d** interconvert on a similar time scale as open-chain APBIs like **2**, as revealed by dynamic NMR spectroscopy. Based on the fact that the spectroscopic data of the diagonally bridged isomers **5a–d** differ significantly from those of reference compound **4**, it can be concluded that conformationally non-restricted APBIs do not exhibit a perpendicular orientation of the aryloxy residues in solution. Instead, based on the observed optical properties of the macrocyclic perylene bisimides **6a–d**, which are similar to reference compound **4**, a conformation with horizontal orientation of the aryloxy groups is given for tetraaryloxy-substituted perylene bisimides such as **4** in solution. The detailed analysis of the absorption and fluorescence properties of isomers **5a–d** showed that the degree of conjugation between the electron-rich aryloxy residue (+M effect) and the electron-poor perylene bisimide core depends on the conformation of the aryloxy residue. Under consideration of the solvent-dependent fluorescence properties of APBIs **4** and macrocycle **5b**, it can be concluded that a photoinduced electron transfer from the electron-rich aryloxy substituent to the electron-deficient perylene core is the most reasonable explanation for the fluorescence quenching of APBIs. Based on these results, it can be proposed that APBIs with high fluorescence quantum yields in polar solvents should bear electron-poor aryloxy residues. Indeed, such fluorophores have recently been introduced by Müllen and co-workers which exhibit high fluorescence quantum yields even in the most polar solvent water.[4b,17a,b]

Experimental Section

Materials and methods: Cesium carbonate (99%) purchased from Aldrich (Steinheim, Germany) and dry DMSO (SeccoSolv) obtained from Merck (Hohenbrunn, Germany) were used as received. *N,N′*-Bis(2,6-diisopropylphenyl)-1,6,7,12-tetrachloroperylene-3,4:9,10-tetracarboxylic acid bisimide (**1**) was donated from BASF AG. Perylene bisimides **2** and **3**[23] and oligoethylene glycol ditosylates[37] were synthesized according to literature procedures.

Flash column chromatography was performed using silica gel Si60 (40–63 μm) from Merck (Hohenbrunn, Germany). Melting points were determined on an Olympus Bx41 polarization microscope and are uncorrect-

ed. ^{1}H NMR spectra were recorded on Bruker Advance 400 and calibrated to the internal standard TMS or the residual solvent peak. MALDI-TOF mass spectra were recorded on a Bruker-Franzen Reflex EA240 instrument and high resolution mass spectra on an ESI MicrOTOF Focus from Bruker Daltonics. Analytical HPLC was performed on a system (PU 2080 PLUS) with a diode array detector (MD 2015) from JASCO equipped with a ternary gradient unit (LG 2080–02) and line-degasser (DG-2080-533). Preparative HPLC was done on a system (PU 2080 PLUS) with a diode array detector (UV 2077 PLUS) from JASCO. HPLC grade solvents (Rectapur) from VWR (Darmstadt, Germany) were used. As column Nucleodur 100–7 C18 ec (Macherey-Nagel; Düren, Germany) was used in the analytical ($\varnothing = 4.6$ mm) as well as semi-preparative ($\varnothing = 21 \times 250$ mm) HPLC.

Temperature-dependent ^{1}H NMR spectroscopy: Temperature-dependent NMR spectroscopy was performed on a Bruker Advance DMX 600 and the spectra referred to the residual solvent peak. Solutions used for high temperature ^{1}H NMR spectroscopy were degassed by three freeze–pump–thaw cycles and the tubes were molten under vacuum (10^{-3} mbar). The temperature was calibrated to the temperature dependent chemical shift of methanol. Coalescence temperatures were determined from spectral broadening and the data evaluated using the coalescence method according to Equations (1) and (2).

Spectroscopy: For all spectroscopic measurements, spectroscopic grade solvents (Uvasol) from Merck (Hohenbrunn, Germany) were used. UV/Vis spectra were recorded on a Perkin Elmer UV/Vis spectrometer Lamda 40P and fluorescence spectra with a PTI QM-4/2003. All fluorescence measurements were performed under aerobic conditions and fluorescence spectra are corrected. The fluorescence quantum yields were determined as the average value for three different excitation wavelengths using *N*,*N*′-bis(2,6-diisopropylphenyl)-1,6,7,12-tetraphenoxyperylene-3,4:9,10-tetracarboxylic acid bisimide as reference ($\Phi_{fl} = 0.96$ in chloroform) by applying high dilution conditions (Abs. < 0.05).[3,38] Fluorescence lifetimes were determined with a PTI GL3330 nitrogen laser and a GL302 dye laser. Decay curves were evaluated with the Felix Software from PTI by fitting 1–4 lifetimes. The quality of the fit was judged by Derbin–Watson factor DW and χ^2 (for monoexponential decay DW > 1.7 and $0.9 < \chi^2 < 1.2$) as well as by the correlation function and the residuals.

Cyclic voltammetry: Cyclic voltammetry was performed on a standard commercial electrochemical analyzer (EC epsilon; BAS Instruments, UK) in a three electrode single-compartment cell under argon. Dichloromethane (HPLC grade) was obtained from J. T. Baker (Mumbai, India) and dried over calcium hydride and degassed prior to use. The supporting electrolyte tetrabutylammonium hexafluorophosphate (TBAHFP) was synthesized according to literature,[39] recrystallized from ethanol/water and dried in high vacuum. The measurements were carried out under exclusion of air and moisture at a concentration of 10^{-4} M with ferrocene as internal standard for the calibration of the potential. Working electrode: Pt disc; reference electrode: Ag/AgCl; auxiliary electrode: Pt wire.

Computational details: The geometries of **2** (bearing methyl as imide substituent) were optimized using MM2 force field with the parameter given in CaChe quantum CaChe workspace 5.0. The dihedral angle was adjusted and fixed before the geometrical optimization and read out after optimization. The calculation was done for twist angles in the range of 0–75° and only for one enantiomer (twist angles from 0–(−75°)). The obtained heat of formation was referred to the energetical minimum, plotted against the dihedral angles and fitted with Equation (4) in order to obtain a function which can be used to calculate the population of different conformations.

$$E(\theta) = a|\theta^2| + b|\theta| + c \tag{4}$$

The best fit obtained delivered the parameters $a = 0.08076$, $b = -4.53163$ and $c = 66$. The population in dependence of the dihedral angle θ was calculated for the different conformations according to Boltzmann statistics [Eq. (5)] at a temperature of 293 K and normalized by dividing through the integral of this function Z.[40]

$$P(\theta) = \frac{e^{-E(\theta)/RT}}{Z} \quad \text{and} \quad Z = \int e^{-E(\theta)/RT} d\theta \tag{5}$$

Additionally, the geometries of APBI **2** and diagonally bridged macrocycles **5a–d** were optimized by the semi-empirical AM1 method as implemented in CaChe Quantum CaChe Workspace 5.0.

Synthesis of reference compound 4 and macrocyclic perylene bisimides 5 and 6

***N*,*N*′-Bis(2,6-diisopropylphenyl)-1,6,7,12-tetra(3-[2-(2-[2-(2-methoxy)-ethoxy] ethoxy)ethoxy]phenoxy)perylene-3,4:9,10-tetracarboxylic acid bisimide (4)**: Perylene bisimide **3** (325 mg, 0.28 mmol), 2-(2-[2-(methoxy)-ethoxy]ethoxy)ethanol tosylate (540 mg, 1.71 mmol) and cesium carbonate (1390 mg, 4.26 mmol) were suspended under argon in dry DMSO (90 mL) and heated at 80 °C for 5 h. The reaction mixture was cooled to room temperature, dropped to a stirred mixture of water (150 mL) and 1 N HCl (150 mL) and after 2 h the resulting precipitate was collected by vacuum filtration and dried at RT over silica gel. Flash column chromatography on silica gel eluting with ethyl acetate with a gradient of 5% methanol and reprecipitation from dichloromethane and *n*-hexane afforded a wine-red solid (135 mg, 28%). M.p. > 300 °C; ^{1}H NMR ($CDCl_3$, 25 °C): $\delta = 8.27$ (s, 4H; CH), 7.43 (t, $^3J(H,H) = 8.0$ Hz, 2H; CH), 7.28 (d, $^3J(H,H) = 8.0$ Hz, 4H; CH), 7.17 (t, $^3J(H,H) = 8.0$ Hz, 4H; CH), 6.68 (ddd, $^3J(H,H) = 8.0$, $^4J(H,H) = 2.5$, $^4J(H,H) = 1.0$ Hz, 4H; CH), 6.60 (ddd, $^3J(H,H) = 8.0$, $^4J(H,H) = 2.5$, $^4J(H,H) = 1.0$ Hz, 4H; CH), 6.53 (t, $^4J(H,H) = 2.5$ Hz, 4H; CH), 3.97 (br t, $^3J(H,H) = 5.0$ Hz, 8H; CH_2), 3.78 (br t, $^3J(H,H) = 5.0$ Hz, 8H; CH_2), 3.70–3.51 (m, 32H; CH_2), 3.35 (s, 12H), 2.71 (sept, $^3J(H,H) = 7.0$ Hz, 4H; CH), 1.13 ppm (d, $^3J(H,H) = 7.0$ Hz, 24H; CH_3); MS (MALDI-TOF, dithranol): *m*/*z*: calcd for: 1727.0; found: 1727.0 $[M+H]^+$, 1740.0 $[M+Na]^+$, 1756.0 $[M+K]^+$; elemental analysis calcd (%) for $C_{76}H_{63}N_2O_{12}\cdot 2H_20$: C 68.09, H 6.74, N 1.59; found: C 68.14, H 6.47, N 1.65; UV/Vis (CH_2Cl_2): λ_{max} (ε_{max}) = 575 (46600), 537 (29800), 448 nm (16600 M^{-1} cm^{-1}); fluorescence (CH_2Cl_2): $\lambda_{max} = 609$ nm, fluorescence quantum yield $\Phi_{fl} = 0.89$, fluorescence lifetime $\tau_{fl} = 5.6$ ns ($\lambda_{ex} = 520$, $\lambda_{em} = 605$ nm); CV (CH_2Cl_2, 0.1 M TBAHFP, 100 mV s^{-1}): $E(PBI/PBI^-) = -1.14$, $E(PBI^-/PBI^{2-}) = -1.35$, $E(PBI/PBI^+) = 0.91$ V.

General procedure for macrocyclisation: Perylene bisimide **3** (1 equiv), cesium carbonate (16 equiv) and the corresponding oligoethylene glycol ditosylates (5–6 equiv) were suspended under argon in DMSO and heated for 5 h at 100 °C. The reaction mixture was cooled to room temperature and dropped under stirring to 0.33 M hydrochloric acid (150 mL). The resulting precipitate was collected by filtration and dried in vacuum. The crude product was applied on silica gel column chromatography and the resulting macrocycles were isolated by precipitation from dichloromethane with a polar or non-polar solvent. The precipitate was collected by filtration and dried in vacuum (10^{-3} mbar) at 60 °C.

Macrocycles 5a and 6a: Macrocycles **5a** and **6a** were synthesized according to the general procedure by the reaction of **3** (410 mg, 0.36 mmol) with ethylene glycol ditosylate (820 mg, 2.21 mmol) in the presence of cesium carbonate (1.92 g, 5.90 mmol) in DMSO (65 mL). Column chromatography on silica gel eluting with dichloromethane and re-precipitation from dichloromethane and methanol yielded **5a** as an orange solid (4.1 mg, 3.43 μmol, 1%) and **6a** as an orange-red solid (22.9 mg, 19.2 μmol, 5%).

Macrocycle 5a: M.p. 423–425 °C; ^{1}H NMR (400 MHz, $CDCl_3$, 30 °C, TMS): $\delta = 8.37$ (s, 4H; CH), 7.50 (t, $^3J(H,H) = 7.7$ Hz, 2H; CH), 7.35 (d, $^3J(H,H) = 7.7$ Hz, 4H; CH), 7.19–7.13 (m, 8H; CH), 6.37 (dd, $^3J(H,H) = 7.6$, $^4J(H,H) = 1.9$ Hz, 4H; CH), 5.27 (t, $^4J(H,H) = 2.2$ Hz, 4H; CH), 3.69 (m, 4H; CH_2), 3.48 (m, 4H; CH_2), 2.72 (sept, $^3J(H,H) = 6.9$ Hz, 4H; CH), 1.21, 1.19 ppm (d, $^3J(H,H) = 6.9$ Hz, 24H; CH_3); (400 MHz, CD_2Cl_2, 30 °C): $\delta = 8.35$ (s, 4H; CH), 7.44 (t, $^3J(H,H) = 7.8$ Hz, 2H; CH), 7.27 (d, $^3J(H,H) = 7.6$ Hz, 4H; CH), 7.05 (m, 8H; CH), 6.28 (m, 4H; CH), 3.56 (m, 4H; CH_2), 3.40 (m, 4H; CH_2), 2.62 (sept, $^3J(H,H) = 6.8$ Hz, 4H; CH), 1.09, 1.06 ppm (d, $^3J(H,H) = 6.8$ Hz, 24H; CH_3); MS (MALDI-TOF, pos. mode, dithranol): *m*/*z*: calcd for: 1194.4; found: 1195.6 $[M+H]^+$; HRMS (ESI-TOF, pos. mode, CH_2Cl_2/acetonitrile 1:1): *m*/*z*: calcd for $C_{76}H_{63}N_2O_{12}$: 1195.4376; found: 1195.4360 $[M+H]^+$; UV/Vis (CH_2Cl_2): λ_{max} (ε_{max}) = 544 (43500), 505 (27600), 474 (14100, sh), 436 (11600),

278 nm (42000 $M^{-1}cm^{-1}$); fluorescence (CH_2Cl_2): $\lambda_{max}=562$ nm; fluorescence quantum yield $\Phi_{fl}=0.02$, fluorescence lifetime $\tau_{fl} < 0.5$ ns ($\lambda_{ex}=520$ nm, $\lambda_{em}=580$ nm); CV (CH_2Cl_2, 0.1 M TBAHFP, 100 $mV s^{-1}$): $E(PBI/PBI^-)=-0.97$, $E(PBI^-/PBI^{2-})=-1.30$ V.

Macrocycle 6a: M.p. >500 °C; ^1H NMR (400 MHz, $CDCl_3$, 30 °C, TMS): $\delta=8.47$ (s, 4H; CH), 7.45 (t, $^3J(H,H)=7.7$ Hz, 2H; CH), 7.30 (d, $^3J(H,H)=7.7$ Hz, 4H; CH), 7.17 (t, $^3J(H,H)=8.1$ Hz, 4H; CH), 6.71 (d, $^3J(H,H)=8.3$ Hz, 4H; CH), 6.48 (t, $^4J(H,H)=2.3$ Hz, 4H; CH), 6.43 (dd, $^3J(H,H)=7.6$, $^4J(H,H)=1.9$, 4H; CH), 4.43 (s, 8H; CH_2), 2.72 (sept, $^3J(H,H)=6.9$ Hz, 4H; CH), 1.16, 1.13 ppm (d, $^3J(H,H)=6.9$ Hz, 24H; CH_3); (400 MHz, CD_2Cl_2, 30 °C): $\delta=8.36$ (s, 4H, CH), 7.39 (t, $^3J(H,H)=7.8$ Hz, 2H; CH), 7.23 (d, $^3J(H,H)=7.8$ Hz, 4H; CH), 7.10 (t, $^3J(H,H)=8.2$ Hz, 4H; CH), 6.65 (ddd, $^3J(H,H)=8.3$, $^4J(H,H)=2.4$, $^4J(H,H)=0.9$ Hz, 4H; CH), 6.36 (m, 8H, CH), 4.36 (s, 8H, CH_2), 2.63 (sept, $^3J(H,H)=6.8$ Hz, 4H; CH), 1.03, 1.00 ppm (d, $^3J(H,H)=6.8$ Hz, 24H; CH_3); MS (MALDI-TOF, pos. mode, dithranol): *m/z*: calcd for: 1194.4; found: 1195.6 $[M+H]^+$; HRMS (ESI-TOF, pos. mode, CH_2Cl_2/acetonitrile 1:1): *m/z*: calcd for $C_{76}H_{63}N_2O_{12}$: 1195.4376; found: 1195.4375 $[M+H]^+$; UV/Vis (CH_2Cl_2): λ_{max} (ε_{max}) 554 (43600), 517 (28600), 448 (14500), 284 (50100), 263 nm (38000 $M^{-1}cm^{-1}$); fluorescence (CH_2Cl_2): $\lambda_{max}=588$ nm, fluorescence quantum yield $\Phi_{fl}=0.78$, fluorescence lifetime $\tau_{fl}=5.4$ ns ($\lambda_{ex}=520$ nm, $\lambda_{em}=600$ nm); CV (CH_2Cl_2, 0.1 M TBAHFP, 100 $mV s^{-1}$): $E(PBI/PBI^-)=-1.07$, $E(PBI^-/PBI^{2-})=-1.32$, $E(PBI/PBI^+)=+1.05$ V.

Macrocycles 5b and 6b: Perylene bisimide **3** (220 mg, 0.19 mmol), diethylene glycol ditosylate (435 mg, 1.05 mmol), and cesium carbonate (713 mg, 2.19 mmol) were reacted according to the general procedure in DMSO (30 mL). The two regioisomers were separated by silica gel column chromatography with dichloromethane and precipitation with methanol afforded **5b** (17.1 mg, 13.3 μmol, 7%) as an orange solid and **6b** (37.0 mg, 28.8 μmol, 15%) as red powder.

Compound 5b: M.p. 374–376 °C; ^1H NMR (400 MHz, $CDCl_3$, 30 °C, TMS): $\delta=8.32$ (s, 4H; CH), 7.47 (t, $^3J(H,H)=7.5$ Hz, 2H; CH), 7.33 (d, $^3J(H,H)=7.5$ Hz, 4H; CH), 7.22 (t, $^3J(H,H)=8.3$ Hz, 4H; CH), 7.16 (ddd, $^3J(H,H)=8.3$, $^4J(H,H)=2.3$, $^4J(H,H)=0.8$ Hz, 4H; CH), 6.46 (ddd, $^3J(H,H)=8.3$, $^4J(H,H)=2.3$, $^4J(H,H)=0.8$ Hz, 4H; CH), 5.73 (t, $^3J(H,H)=2.3$ Hz, 4H; CH), 3.94–3.89 (m, 4H; CH), 3.72–3.64 (m, 8H; CH), 3.58–3.55 (m, 4H; CH), 2.82 (sept, $^3J(H,H)=6.9$ Hz, 4H; CH), 1.19, 1.17 ppm (d, $^3J(H,H)=6.9$ Hz, 24H; CH_3); (400 MHz, CD_2Cl_2, 30 °C): $\delta=8.32$ (s, 4H; CH), 7.48 (t, $^3J(H,H)=7.6$ Hz, 2H; CH), 7.31 (m, 8H; CH), 7.20 (ddd, $^3J(H,H)=8.2$, $^4J(H,H)=2.3$, $^4J(H,H)=0.9$ Hz, 4H; CH), 6.49 (ddd, $^3J(H,H)=8.2$, $^4J(H,H)=2.3$, $^4J(H,H)=0.9$ Hz, 4H; CH), 5.72 (t, $^3J(H,H)=2.3$, 4H; CH), 3.85–3.80 (m, 4H; CH_2), 3.70–3.50 (m, 12H; CH_2), 2.72 (sept, $^3J(H,H)=6.8$, 4H; CH), 1.11, 1.09 ppm (d, $^3J(H,H)=6.8$ Hz, 24H; CH_3); MS (MALDI-TOF, pos. mode, dithranol): *m/z*: calcd for: 1282.5; found: 1283.8 $[M+H]^+$; HRMS (ESI-TOF, pos. mode, CH_2Cl_2/acetonitrile 1:1): *m/z*: calcd for $C_{80}H_{71}N_2O_{14}$: 1283.4900; found: 1283.4898 $[M+H]^+$, 1305.4713 $[M+Na]^+$; UV/Vis (CH_2Cl_2): λ_{max} (ε_{max}) = 534 (41700), 499 (27500), 467 (14500), 436 (11600), 265 nm (42000 $M^{-1}cm^{-1}$); fluorescence (CH_2Cl_2): $\lambda_{max}=573$ nm, fluorescence quantum yield $\Phi_{fl}=0.09$, fluorescence lifetime $\tau_{fl}=0.8$ ns ($\lambda_{ex}=520$, $\lambda_{em}=580$ nm); CV (CH_2Cl_2, 0.1 M TBAHFP, 100 $mV s^{-1}$): $E(PBI/PBI^-)=-1.06$, $E(PBI^-/PBI^{2-})=-1.38$, $E(PBI/PBI^+)=+1.16$ V.

Compound 6b: M.p. 365–367 °C; ^1H NMR (400 MHz, $CDCl_3$, 30 °C, TMS): $\delta=8.38$ (s, 4H; CH), 7.43 (t, $^3J(H,H)=7.8$ Hz, 2H; CH), 7.28 (d, $^3J(H,H)=7.8$ Hz, 4H; CH), 7.08 (t, $^3J(H,H)=8.3$ Hz, 4H; CH), 6.72 (dd, $^3J(H,H)=7.6$, $^3J(H,H)=1.9$ Hz, 4H; CH), 6.60–6.55 (m, 8H; CH), 4.18 (brs, 8H; CH_2), 3.94 (brs, 4H; CH_2), 3.79 (brs, 4H; CH_2), 2.71 (sept, $^3J(H,H)=6.8$ Hz, 4H; CH), 1.14 ppm (brs, 24H; CH_2); MS (MALDI-TOF, pos. mode, dithranol): *m/z*: calcd for: 1282.5; found: 1283.7 $[M+H]^+$; HRMS (ESI-TOF, pos. mode, CH_2Cl_2/acetonitrile 1:1): *m/z*: calcd for $C_{80}H_{71}N_2O_{14}$: 1283.4900; found: 1283.4850 $[M+H]^+$, 1305.4723 $[M+Na]^+$; UV/Vis (CH_2Cl_2): λ_{max} (ε_{max}) = 576 (46700), 536 (28600), 451 (15400), 285 (48800), 265 nm (37500 $M^{-1}cm^{-1}$); fluorescence (CH_2Cl_2): $\lambda_{max}=605$ nm, fluorescence quantum yield $\Phi_{fl}=0.82$, fluorescence lifetime $\tau_{fl}=5.3$ ns ($\lambda_{ex}=520$, $\lambda_{em}=600$ nm); CV (CH_2Cl_2, 0.1 M TBAHFP, 100 $mV s^{-1}$): $E(PBI/PBI^-)=-1.11$, $E(PBI^-/PBI^{2-})=-1.30$, $E(PBI/PBI^+)=+0.91$ V.

Macrocycles 5c and 6c: The macrocycles **5c** and **6c** were synthesized according to the general procedure by the reaction of **3** (197 mg, 0.17 mmol) with triethylene glycol ditosylate (518 mg, 1.03 mmol) in the presence of cesium carbonate (900 mg, 2.72 mmol) in DMSO (30 mL). After column chromatographic purification on silica gel with dichloromethane (0.3% methanol) and reprecipitation from dichloromethane with methanol, **5c** (4.7 mg, 1.60 μmol, 2%) was obtained as an orange solid and **6c** as wine-red solid (21.1 mg, 15.3 μmol, 8%).

Compound 5c: M.p. 370–372 °C; ^1H NMR (400 MHz, $CDCl_3$, 30 °C, TMS): $\delta=8.29$ (s, 4H; CH), 7.45 (t, $^3J(H,H)=7.7$ Hz, 2H; CH), 7.32–7.30 (m, 8H; CH), 7.14 (dd, $^3J(H,H)=8.0$, $^4J(H,H)=2.3$ Hz, 4H; CH), 6.56 (dd, $^3J(H,H)=8.0$, $^4J(H,H)=2.2$ Hz, 4H; CH), 6.03 (t, $^4J(H,H)=2.3$ Hz, 4H; CH), 3.93–3.88 (m, 4H; CH_2), 3.79–3.74 (m, 4H; CH_2), 3.69–3.50 (m, 16H; CH_2), 2.77 (sept, $^3J(H,H)=6.9$ Hz, 4H; CH), 1.16, 1.14 ppm (d, $^3J(H,H)=6.4$ Hz, 24H; CH_3); (400 MHz, CD_2Cl_2, 30 °C): $\delta=8.28$ (s, 4H; CH), 7.47 (t, $^3J(H,H)=7.6$ Hz, 2H; CH), 7.38 (t, $^3J(H,H)=8.2$ Hz, 4H; CH), 7.30 (d, $^3J(H,H)=7.8$ Hz, 4H; CH), 7.21 (ddd, $^3J(H,H)=8.4$, $^4J(H,H)=2.3$, $^4J(H,H)=0.8$ Hz, 4H; CH), 6.61 (ddd, $^3J(H,H)=8.4$, $^4J(H,H)=2.4$, $^4J(H,H)=0.9$ Hz, 4H; CH), 6.09 (t, $^4J(H,H)=2.4$ Hz, 4H; CH), 3.93–3.87 (m, 4H; CH_2), 3.83–3.78 (m, 4H; CH_2), 3.67–3.56 (m, 16H; CH_2), 2.77 (sept, $^3J(H,H)=6.8$ Hz, 4H; CH), 1.16, 1.14 ppm (d, $^3J(H,H)=6.8$ Hz, 24H; CH_3); MS (MALDI-TOF, pos. mode, dithranol): *m/z*: calcd for: 1370.5; found: 1371.8 $[M+H]^+$; HRMS (APCI, pos. mode, chloroform): *m/z*: calcd for $C_{84}H_{79}N_2O_{16}$: 1371.5424; found: 1371.5440 $[M+H]^+$; UV/Vis (CH_2Cl_2): λ_{max} (ε_{max}) = 545 (37700), 513 (26500, sh), 449 (13700), 281 nm (42800 $M^{-1}cm^{-1}$); fluorescence (CH_2Cl_2): $\lambda_{max}=582$ nm, fluorescence quantum yield $\Phi_{fl}=0.43$, fluorescence lifetime $\tau_{fl}=2.7$ ns ($\lambda_{ex}=520$, $\lambda_{em}=580$ nm); CV (CH_2Cl_2, 0.1 M TBAHFP, 100 $mV s^{-1}$): $E(PBI/PBI^-)=-1.13$, $E(PBI^-/PBI^{2-})=-1.39$, $E(PBI/PBI^+)=+1.09$ V.

Compound 6c: M.p. 314–315 °C; ^1H NMR (400 MHz, $CDCl_3$, 30 °C, TMS): $\delta=8.30$ (s, 4H; CH), 7.43 (t, $^3J(H,H)=7.8$ Hz, 2H; CH), 7.27 (d, $^3J(H,H)=7.8$ Hz, 4H; CH), 7.13 (t, $^3J(H,H)=8.2$ Hz, 4H; CH), 6.70 (t, $^3J(H,H)=2.4$ Hz, 4H; CH), 6.65 (ddd, $^3J(H,H)=8.4$, $^4J(H,H)=2.4$, $^4J(H,H)=0.8$ Hz, 4H; CH), 6.56 (ddd, $^3J(H,H)=8.2$, $^4J(H,H)=2.2$, $^4J(H,H)=0.8$ Hz, 4H; CH), 4.07–4.02 (m, 8H; CH_2), 3.85 (brs, 8H; CH_2), 3.79–3.73 (m, 8H; CH_2), 2.71 (sept, $^3J(H,H)=6.8$ Hz, 4H; CH), 1.13 (brd, $^3J(H,H)=6.8$ Hz, 24H; CH_3); (400 MHz, CD_2Cl_2, 30 °C), $\delta=8.21$(s, 4H; CH), 7.47 (t, $^3J(H,H)=7.8$ Hz, 2H; CH), 7.27 (d, $^3J(H,H)=7.8$ Hz, 4H; CH), 7.20 (t, $^3J(H,H)=8.1$ Hz, 4H; CH), 6.73 (m, 8H; CH), 6.58 (ddd, $^3J(H,H)=8.1$, $^4J(H,H)=2.3$, $^4J(H,H)=0.8$ Hz, 4H; CH), 4.03 (m, 8H; CH_2), 3.81 (m, 8H; CH_2), 3.68 (m, 8H; CH_2), 2.70 (sept, $^3J(H,H)=6.8$ Hz, 4H; CH), 1.09 (d, $^3J(H,H)=6.8$ Hz, 24H; CH_3); MS (MALDI-TOF, pos. mode, dithranol): *m/z*: calcd for: 1370.5; found: 1371.9 $[M+H]^+$; HRMS (ESI-TOF, pos. mode, CH_2Cl_2/acetonitrile 1:1): *m/z*: calcd for $C_{84}H_{78}N_2O_{16}Na$: 1393.5203; found: 1393.5245 $[M+Na]^+$; UV/Vis (CH_2Cl_2): λ_{max} (ε_{max}) = 580 (49400), 539 (29900), 450 (16600), 287 (53500), 268 nm (43300 $M^{-1}cm^{-1}$); fluorescence (CH_2Cl_2): $\lambda_{max}=606$ nm, fluorescence quantum yield $\Phi_{fl}=0.84$, fluorescence lifetime $\tau_{fl}=5.6$ ns ($\lambda_{ex}=520$, $\lambda_{em}=600$ nm); CV (CH_2Cl_2, 0.1 M TBAHFP, 100 $mV s^{-1}$): $E(PBI/PBI^-)=-1.14$, $E(PBI^-/PBI^{2-})=-1.35$, $E(PBI/PBI^+)=+0.90$.

Macrocycles 5d and 6d: Perylene bisimide **3** (197 mg, 0.17 mmol), tetraethylene glycol ditosylate (518 mg, 1.03 mmol), and cesium carbonate (900 mg, 2.72 mmol) were reacted in DMSO (30 mL) according to the general procedure. The two isomeric macrocycles were separated by silica gel column chromatography with dichloromethane and a gradient of 0.3–1% of methanol. Additional purification by HPLC (Nucleodur 100–7 C18 ec, eluent: methanol) of the first eluted fraction and precipitation with *n*-hexane afforded **5d** (7.2 mg, 4.93 μmol; l3.3%) as orange solid. Column chromatography of the second eluted fraction with dichloromethane (0.5% methanol) and reprecipitation from dichloromethane and methanol yielded **6d** (12.8 mg, 8.76 μmol, 5%) as a red solid.

Compound 5d: M.p. 372–374 °C; retention time t_R (Nucleodur 100–7 C18 ec, methanol, 1 mL min^{-1}) = 10.8 min; ^1H NMR (400 MHz, $CDCl_3$, 30 °C, TMS): $\delta=8.26$ (s, 4H; CH), 7.45 (t, $^3J(H,H)=7.8$ Hz, 2H; CH), 7.30 (m, 8H; CH), 7.01 (ddd, $^3J(H,H)=8.2$, $^4J(H,H)=2.3$, $^4J(H,H)=0.8$ Hz, 4H; CH), 6.61 (ddd, $^3J(H,H)=8.3$, $^4J(H,H)=2.4$, $^4J(H,H)=0.8$ Hz, 4H; CH), 6.20 (t, $^4J(H,H)=2.3$ Hz, 4H; CH), 3.99–3.93 (m, 4H; CH_2), 3.87–3.82

(m, 4H; CH_2), 3.68–3.66 (m, 8H; CH_2), 3.58–3.56 (m, 16H; CH_2), 2.75 (sept, ^3J(H,H) = 6.8 Hz, 4H; CH), 1.14, 1.14 ppm (d, ^3J(H,H) = 6.8 Hz, 24H; CH_3); (400 MHz, CD_2Cl_2, 30 °C): δ = 8.21 (s, 4H; CH), 7.42 (t, ^3J(H,H) = 7.8 Hz, 2H; CH), 7.36–7.30 (m, 8H; CH), 7.05 (ddd, ^3J(H,H) = 8.1, ^4J(H,H) = 2.3, ^4J(H,H) = 0.8 Hz, 4H; CH), 6.65 (ddd, ^3J(H,H) = 8.3, ^4J(H,H) = 2.3, ^4J(H,H) = 0.8 Hz, 4H; CH), 6.24 (t, ^4J(H,H) = 2.3 Hz, 4H; CH), 3.96–3.91 (m, 4H; CH_2), 3.86–3.81 (m, 4H; CH_2), 3.64–3.61 (m, 8H; CH_2), 3.52–3.45 (m, 16H; CH_2), 2.70 (sept, ^3J(H,H) = 6.8 Hz, 4H; CH), 1.09 ppm (d, ^3J(H,H) = 6.8 Hz, 24H; CH_3); MS (MALDI-TOF, pos. mode, dithranol): *m/z*: calcd for: 1458.6; found: 1459.6 $[M+H]^+$; HRMS (ESI-TOF, pos. mode, CH_2Cl_2/acetonitrile 1:1): *m/z*: calcd for $C_{88}H_{87}N_2O_{18}$: 1459.5948; found: 1459.5962 $[M+H]^+$; UV/Vis (CH_2Cl_2): λ_{max} (ε_{max}) = 558 (46700), 521 (30800), 450 (15700), 288 (54300), 278 nm (41500 $M^{-1}cm^{-1}$); fluorescence (CH_2Cl_2): λ_{max} = 588 nm, fluorescence quantum yield Φ_{fl} = 0.90, fluorescence lifetime τ_{fl} = 5.5 ns (λ_{ex} = 520, λ_{em} = 580 nm); CV (CH_2Cl_2, 0.1 M TBAHFP, 100 mV s^{-1}): E(PBI/PBI$^-$) = −1.17, E(PBI$^-$/PBI^{2-}) = −1.39, E(PBI/PBI$^+$) = +0.98 V.

Compound 6d: M.p. 314–315 °C; ^{1}H NMR (400 MHz, $CDCl_3$, 30 °C, TMS): δ = 8.27 (s, 4H; CH), 7.43 (t, ^3J(H,H) = 7.7 Hz, 2H; CH), 7.28–7.27 (m, 4H; CH), 7.15 (t, ^3J(H,H) = 8.3 Hz, 4H; CH), 6.69 (d, ^3J(H,H) = 8.5 Hz, 4H; CH), 6.60–6.57 (m, 8H; CH), 3.93–3.87 (br m, 16H; CH_2), 3.71 (br s, 16H; CH_2), 2.71 (sept, ^3J(H,H) = 6.8 Hz, 4H; CH), 1.12 ppm (d, ^3J(H,H) = 6.3 Hz, 24H; CH_3); (400 MHz, CD_2Cl_2, 30 °C): δ = 8.21 (s, 4H; CH), 7.46 (t, ^3J(H,H) = 7.7 Hz, 2H; CH), 7.31 (d, ^3J(H,H) = 7.7 Hz, 4H; CH), 7.20 (t, ^3J(H,H) = 8.4 Hz, 4H; CH), 6.74 (ddd, ^3J(H,H) = 8.4, ^4J(H,H) = 2.3, ^4J(H,H) = 1.0 Hz, 4H; CH), 6.64–6.60 (m, 8H; CH), 3.94 (br s, 8H; CH_2), 3.82 (br m, 8H; CH_2) 3.70–3.63 (br m, 16H; CH_2), 2.70 (sept, ^3J(H,H) = 6.8 Hz, 4H; CH), 1.10 ppm (d, ^3J(H,H) = 6.8 Hz, 24H; CH_3); MS (MALDI-TOF, pos. mode, dithranol): *m/z*: calcd for: 1458.6; found: 1459.8 $[M+H]^+$; HRMS (ESI-TOF, pos. mode, CH_2Cl_2/acetonitrile 1:1): *m/z*: calcd for $C_{88}H_{87}N_2O_{18}$: 1459.5948, found: 1459.5975 $[M+H]^+$; UV/Vis (CH_2Cl_2): λ_{max} (ε_{max}) = 577 (49200), 537 (30100), 449 (17200), 285 (51200), 267 nm (40400 $M^{-1}cm^{-1}$); fluorescence (CH_2Cl_2): λ_{max} = 606 nm, fluorescence quantum yield Φ_{fl} = 0.82, fluorescence lifetime τ_{fl} = 5.5 ns (λ_{ex} = 520, λ_{em} = 600 nm); CV (CH_2Cl_2, 0.1 M TBAHFP, 100 mV s^{-1}): E(PBI/PBI$^-$) = −1.14, E(PBI$^-$/PBI^{2-}) = −1.36, E(PBI/PBI$^+$) = +0.90 V.

Acknowledgements

We cordially thank Mrs. E. Ruckdeschel and Dr. M. Grüne for measuring the temperature-dependent ^{1}H NMR spectra, and the DFG and the Fonds der Chemischen Industrie for financial support of our work.

[1] a) G. Seybold, G. Wagenblast, *Dyes Pigm.* **1987**, *11*, 303–317; b) G. Seybold, A. Stange (BASF AG), Ger. Pat., DE 3545004, **1987** (*Chem. Abstr.* **1988**, *108*, 77134c).

[2] a) F. Würthner, *Chem. Commun.* **2004**, 1564–1579; b) A. C. Grimsdale, K. Müllen, *Angew. Chem.* **2005**, *117*, 5732–5772; *Angew. Chem. Int. Ed.* **2005**, *44*, 5592–5629; c) F. Würthner, *Pure Appl. Chem.* **2006**, *78*, 2341–2350; d) M. R. Wasielewski, *J. Org. Chem.* **2006**, *71*, 5051–5066.

[3] R. Gvishi, R. Reisfeld, Z. Burshstein, *Chem. Phys. Lett.* **1993**, *213*, 338–344.

[4] a) T. D. M. Bell, S. Habuchi, S. Masuo, I. Österling, K. Müllen, P. Tinnefeld, M. Sauer, M. van der Auweraer, J. Hofkens, F. C. De Schryver, *Aust. J. Chem.* **2004**, *57*, 1169–1173; b) A. Margineanu, J. Hofkens, M. Cotlet, S. Habuchi, A. Stefan, J. Qu, C. Kohl, K. Müllen, J. Vercammen, Y. Engelborghs, T. Gensch, F. C. De Schryver, *J. Phys. Chem. B* **2004**, *108*, 12242–12251; c) F. C. De Schryver, T. Vosch, M. Cotlet, M. van der Auweraer, K. Müllen, J. Hofkens, *Acc. Chem. Res.* **2005**, *38*, 514–522; d) E. Lang, F. Würthner, J. Köhler, *ChemPhysChem* **2005**, *6*, 935–941; E. Lang, F. Würthner, J. Köhler, *ChemPhysChem* **2006**, *7*, 292.

[5] For OLEDs, see: a) P. Ranke, I. Bleyl, J. Simmer, D. Haarer, A. Bacher, H. W. Schmidt, *Appl. Phys. Lett.* **1997**, *71*, 1332–1334; b) P. Pösch, M. Thelakkat, H. W. Schmidt, *Synth. Met.* **1999**, *102*, 1110–1112; c) F. Würthner, C. Thalacker, S. Diele, C. Tschierske, *Chem. Eur. J.* **2001**, *7*, 2245–2253; d) L. Fan, W. Zhu, J. Li, H. Tian, *Synth. Met.* **2004**, *145*, 203–210; for PLEDs, see: e) C. Ego, D. Marsitzky, S. Becker, J. Zhang, A. C. Grimsdale, K. Müllen, J. D. MacKenzie, C. Silva, R. H. Friend, *J. Am. Chem. Soc.* **2003**, *125*, 437–443.

[6] J. Baggerman, D. C. Jagesar, R. E. Vallée, J. Hofkens, F. C. De Schryver, F. Schelhase, F. Vögtle, A. M. Brouwer, *Chem. Eur. J.* **2007**, *13*, 1291–1299.

[7] a) F. Würthner, A. Sautter, D. Schmidt, P. J. A. Weber, *Chem. Eur. J.* **2001**, *7*, 894–902; b) C.-C. You, F. Würthner, *J. Am. Chem. Soc.* **2003**, *125*, 9716–9725; c) C.-C. You, C. Hippius, M. Grüne, F. Würthner, *Chem. Eur. J.* **2006**, *12*, 7510–7519.

[8] C. Addicott, I. Österling, T. Yamamoto, K. Müllen, P. J. Stang, *J. Org. Chem.* **2005**, *70*, 797–801.

[9] a) R. Dobrawa, M. Lysteska, P. Ballester, M. Grüne, F. Würthner, *Macromolecules* **2005**, *38*, 1315–1325; b) Y. Li, N. Wang, H. Gan, H. Liu, H. Li, Y. Li, X. He, C. Huang, S. Cui, S. Wang, D. Zhu, *J. Org. Chem.* **2005**, *70*, 9686–9692.

[10] a) F. Würthner, B. Hanke, M. Lysetska, G. Lambright, G. S. Harms, *Org. Lett.* **2005**, *7*, 967–970; for organogels based on diaryloxy-substituted perylene bisimides, see: b) K. Sugiyasu, N. Fujita, S. Shinkai, *Angew. Chem.* **2004**, *116*, 1249–1253; *Angew. Chem. Int. Ed.* **2004**, *43*, 1229–1233; c) Y. Liu, Y. Li, H. Gan, H. Liu, Y. Li, J. Zhuang, F. Lu, D. Zhu, *J. Org. Chem.* **2004**, *69*, 9049–9054.

[11] a) Y. Liu, J. Zhuang, H. Liu, Y. Li, F. Lu, H. Gan, T. Jiu, N. Wang, X. He, D. Zhu, *ChemPhysChem* **2004**, *5*, 1210–1215; b) C. Hippius, F. Schlosser, M. O. Vysotsky, V. Böhmer, F. Würthner, *J. Am. Chem. Soc.* **2006**, *128*, 3870–3871; for examples of diaryloxy-substituted perylene bisimides, see: c) A. S. Lukas, Y. Zhao, S. E. Miller, M. R. Wasielwski, *J. Phys. Chem. B* **2002**, *106*, 1299–1306; d) M. J. Ahrens, L. E. Sinks, B. Rybtchinski, W. Liu, B. A. Jones, J. M. Giaimo, A. V. Gusev, A. J. Goshe, D. M. Tiede, M. R. Wasielwski, *J. Am. Chem. Soc.* **2004**, *126*, 8284–8294.

[12] a) D. Liu, S. De Feyter, M. Cotlet, A. Stefan, U.-M. Wiesler, A. Herrmann, D. Grebel-Koehler, J. Qu, K. Müllen, F. C. De Schryver, *Macromolecules* **2003**, *36*, 5918–5925; b) J. Qu, N. G. Pschirer, D. Liu, A. Stefan, F. C. De Schryver, K. Müllen, *Chem. Eur. J.* **2004**, *10*, 528–537; c) C.-C. You, C. R. Saha-Möller, F. Würthner, *Chem. Commun.* **2004**, 2030–2031; d) J. Pan, W. Zhu, S. Li, W. Zeng, Y. Cao, H. Tian, *Polymer* **2005**, *46*, 7658–7669; e) J. Pan, W. Zhu, S. Li, J. Xu, H. Tian, *Eur. J. Org. Chem.* **2006**, 986–1001; f) M. D. Yilmaz, O. A. Bozdemir, E. U. Akkaya, *Org. Lett.* **2006**, *8*, 2871–2873; for a 1,7-disubstituted perylene bisimde, see: g) T. Ishi-i, K.-i. Murakami, Y. Imai, S. Mataka, *J. Org. Chem.* **2006**, *71*, 5752–5760.

[13] a) A. P. H. J. Schenning, J. v. Herrikhuyzen, P. Jonkheijm, Z. Chen, F. Würthner, E. W. Meijer, *J. Am. Chem. Soc.* **2002**, *124*, 10252–10253; b) E. H. A. Beckers, S. C. J. Meskers, A. P. H. J. Schenning, Z. Chen, F. Würthner, P. Marsal, D. Beljonne, J. Cornil, R. A. J. Janssen, *J. Am. Chem. Soc.* **2006**, *128*, 649–657; c) E. H. A. Beckers, Z. Chen, S. C. J. Meskers, P. Jonkheijm, A. P. H. J. Schenning, X.-Q. Li, P. Osswald, F. Würthner, R. A. J. Janssen, *J. Phys. Chem. B* **2006**, *110*, 16967–16978.

[14] a) C.-C. You, F. Würthner, *Org. Lett.* **2004**, *6*, 2401–2404; b) A. Prodi, C. Chiroboli, F. Scandola, E. Iengo, E. Alessio, R. Dobrawa, F. Würthner, *J. Am. Chem. Soc.* **2005**, *127*, 1454–1462; c) N. Wang, F. Lu, C. Huang, Y. Li, M. Yuan, X. Liu, H. Liu, L. Gan, L. Jiang, D. Zhu, *J. Poly. Sci. A* **2006**, *44*, 5863–5874; for examples of diaryloxy-substituted perylene bisimides, see: d) T. van der Boom, R. T. Hayes, Y. Zhao, P. J. Bushard, E. A. Weiss, M. R. Wasielewski, *J. Am. Chem. Soc.* **2002**, *124*, 9582–9590; e) X. He, H. Liu, Y. Li, Y. Liu, F. Lu, Y. Li, D. Zhu, Macromol. *Chem. Phys.* **2005**, *206*, 2199–2205; f) S. Xiao, M. E. El-Khouly, Y. Li, Z. Gan, H. Liu, L. Jiang, Y. Araki, O. Ito, D. Zhu, *J. Phys. Chem. B* **2005**, *109*, 3658–3667.

[15] B. K. Kaletas, R. Dobrawa, A. Sautter, F. Würthner, M. Zimine, L. De Cola, R. M. Williams, *J. Phys. Chem. A* **2004**, *108*, 1900–1909.

[16] a) Y. Liu, S. Xiao, H. Li, Y. Li, H. Liu, F. Lu, J. Zhuang, D. Zhu, *J. Phys. Chem. B* **2004**, *108*, 6256–6260; b) J. Hua, F. Ding F. S. Meng, H. Tian, *Chin. Chem. Lett.* **2004**, *15*, 1373–1376; c) J. Hua, F. Meng, F. Ding, F. Li, H. Tian, *J. Mater. Chem.* **2004**, *14*, 1849–1853; for examples of diaryloxy-substituted perylene bisimides, see: d) Y. Liu, N. Wang, Y. Li, H. Liu, Y. Li, J. Xiao, X. Xu, C. Huang, S. Cui, D. Zhu, *Macromolecules* **2005**, *38*, 4880–4887; e) J. Zhuang, W. Zhou, X. Li, Y. Li, N. Wang, X. He, H. Liu, Y. Li, L. Jiang, C. Huang, S. Cui, S. Wang, D. Zhu, *Tetrahedron* **2005**, *61*, 8686–8693.

[17] a) M. A. Abdalla, J. Bayer, J. O. Rädler, K. Müllen, *Angew. Chem.* **2004**, *116*, 4057–4060; *Angew. Chem. Int. Ed.* **2004**, *43*, 3967–3970; b) C. Kohl, T. Weil, J. Qu, K. Müllen, *Chem. Eur. J.* **2004**, *10*, 5297–5310; c) S. Krauß, M. Lysetska, F. Würthner, *Lett. Org. Chem.* **2005**, *2*, 349–353.

[18] J. Ren, X.-L. Zhao, Q.-C. Wang, C.-F. Ku, D.-H. Qu, C.-P. Chang, H. Tian, *Dyes Pigm.* **2005**, *64*, 193–200.

[19] J. Hofkens, T. Vosch, M. Maus, F. Köhn, M. Cotlet, T. Weil, A. Herrmann, K. Müllen, F. C. De Schryver, *Chem. Phys. Lett.* **2001**, *333*, 255–263.

[20] A. Sautter, C. Thalacker, F. Würthner, *Angew. Chem.* **2001**, *113*, 4557–4560; *Angew. Chem. Int. Ed.* **2001**, *40*, 4425–4428.

[21] a) M. Cotlet, S. Masuo, M. Lor, E. Fron, M. van der Auweraer, K. Müllen, J. Hofkens, F. C. De Schryver, *Angew. Chem.* **2004**, *116*, 6242–6246; *Angew. Chem. Int. Ed.* **2004**, *43*, 6116–6120; b) C. Flors, I. Oesterling, E. Fron, G. Schweitzer, M. Sliwa, A. Herrmann, M. van der Auweraer, F. C. De Schryver, K. Müllen, J. Hofkens, *J. Phys. Chem. C* **2007**, *111*, 4861–4870; for a recent comparison of different diarylsubstituted perylene bisimides, see: c) C.-C. Chao, M.-k. Leung, Y. O. Su, K.-Y. Chiu, T.-H. Lin, S.-J. Shieh, S.-C. Lin, *J. Org. Chem.* **2005**, *70*, 4323–4331.

[22] A part of this work has been communicated: P. Osswald, D. Leusser, D. Stalke, F. Würthner, *Angew. Chem.* **2005**, *117*, 254–257; *Angew. Chem. Int. Ed.* **2005**, *44*, 250–253.

[23] S. Hien, PhD Thesis, University of Regensburg (Germany), **1995**.

[24] a) U. Lüning, M. Müller, *Chem. Ber.* **1990**, *123*, 643–645; b) G. Ferguson, A. J. Lough, A. Notti, S. Pappalardo, M. F. Parasi, A. Petringa, *J. Org. Chem.* **1998**, *63*, 9703–9710; c) J. A. Wisner, P. D. Beer, M. G. B. Drew, *Angew. Chem.* **2001**, *113*, 3718–3721; *Angew. Chem. Int. Ed.* **2001**, *40*, 3610–3612; for a review on macrocyclisation, see: d) P. Knops, N. Sendhoff, H. B. Mekelburger, F. Vögtle, *Top. Curr. Chem.* **1992**, *161*, 1–36.

[25] a) B. Dietrich, P. Viout, J.-M. Lehn, *Macrocyclic Chemistry*, Wiley VCH, Weinheim, **1993**; b) A. Ostrowicki, E. Koepp, F. Vögtle, *Top. Curr. Chem.* **1992**, *161*, 37–67.

[26] a) W. L. Mattice, *Macromolecules* **1979**, *12*, 944–948; b) M. A. Winnik, *Chem. Rev.* **1981**, *81*, 491–524.

[27] M. Hesse, H. Meier, B. Zeeh, *Spectroscopic Methods in Organic Chemistry*, Thieme, Stuttgart, **1997**, pp. 88–100.

[28] K. Müllen, W. Heinz, F.-G. Klärner, W. R. Roth, I. Kindermann, O. Adamczak, M. Wette, J. Lex, *Chem. Ber.* **1990**, *123*, 2349–2371.

[29] a) I. Petterson, K. Gundertofte, *J. Comput. Chem.* **1991**, *12*, 839–843; b) C. Etzlstorfer, H. Falk, N. Müller, *Monatsh. Chem.* **1993**, *124*, 431–439; c) C. Etzlstorfer, H. Falk, N. Müller, W. Schmitzberger, U. G. Wagner, *Monatsh. Chem.* **1993**, *124*, 751–761; d) C. Etzlstorfer, H. Falk, *Monatsh. Chem.* **1993**, *124*, 1031–1039; e) S. S. Yilmaz, R. Abbasoglu, B. Hazer, *J. Mol. Model.* **2003**, *9*, 230–234.

[30] C.-C. You, F. Würthner, *J. Am. Chem. Soc.* **2003**, *125*, 9716–9725.

[31] a) D. Rehm, A. Weller, *Ber. Bunsenges. Phys. Chem.* **1969**, *73*, 834–845; b) A. Weller, *Z. Phys. Chem. (Muenchen Ger.)* **1982**, *133*, 93–98; c) N. P. Redmore, I. V. Rubtsov, M. J. Therien, *J. Am. Chem. Soc.* **2003**, *125*, 8769–8778; d) M. W. Holman, R. Liu, L. Zang, P. Yan, S. A. DiBenedetto, R. D. Bowers, D. A. Adams, *J. Am. Chem. Soc.* **2004**, *126*, 16126–16133.

[32] C.-C. You, R. Dobrawa, C. R. Saha-Möller, F. Würthner, *Top. Curr. Chem.* **2005**, *258*, 39–82.

[33] C. Vande Velde, E. Bultinck, K. Tersago, C. Van Alsenoy, F. Blockhuys, *Int. J. Quantum Chem.* **2007**, *107*, 670–679.

[34] T. H. Goodwin, M. Przybylska, J. M. Robertson, *Acta Crystallogr.* **1950**, *3*, 279–284.

[35] H. J. Talberg, *Acta Chem. Scand.* **1978**, *32*, 373–374.

[36] The electrochemical potentials in dichloromethane have been taken from the following literature and referred to ferrocene by applying the potential of ferrocene (+0.52 V) vs SCE: T. Higuchi, C. Satake, M. Hirobe, *J. Am. Chem. Soc.* **1995**, *117*, 8879–8880.

[37] a) D. Marquis, J.-P. Desvergne, H. Bouas-Laurent, *J. Org. Chem.* **1995**, *60*, 7984–7996; b) S. Chatti, M. Bortolussi, A. Loupy, *Tetrahedron* **2000**, *56*, 5877–5883.

[38] J. R. Lakowitz, *Principles of Flourescence Spectroscopy*, Kluwer Academic/Plenum, New York, 2nd ed., **1999**, pp. 52–55.

[39] A. J. Fry in *Laboratory Techniques in Electroanalytical Chemistry* (Eds.: P. T. Kessing, W. R. Heineman), Marcel Dekker, New York, 2nd ed., **1996**, p. 481.

[40] C. J. Adam, S. J. Clark, G. J. Ackland, J. Crain, *Phys. Rev. E* **1997**, *55*, 5641–5650.

Received: April 19, 2007
Published online: July 18, 2007

